

An on-demand scheme driven by the knowledge of geospatial distribution for large-scale high-resolution impervious surface mapping

Min Huang, Nengcheng Chen, Wenying Du, Mengtian Wen, Daoye Zhu & Jianya Gong

To cite this article: Min Huang, Nengcheng Chen, Wenying Du, Mengtian Wen, Daoye Zhu & Jianya Gong (2021): An on-demand scheme driven by the knowledge of geospatial distribution for large-scale high-resolution impervious surface mapping, *GIScience & Remote Sensing*, DOI: [10.1080/15481603.2021.1909304](https://doi.org/10.1080/15481603.2021.1909304)

To link to this article: <https://doi.org/10.1080/15481603.2021.1909304>



Published online: 13 Apr 2021.



Submit your article to this journal



View related articles



CrossMark

View Crossmark data



An on-demand scheme driven by the knowledge of geospatial distribution for large-scale high-resolution impervious surface mapping

Min Huang ^a, Nengcheng Chen ^{a,b,c}, Wenying Du ^{a,c}, Mengtian Wen^a, Daoye Zhu^d and Jianya Gong^{a,b,e}

^aState Key Laboratory of Information Engineering in Surveying, Mapping, and Remote Sensing, Wuhan University, Wuhan, China;

^bCollaborative Innovation Center of Geospatial Technology, Wuhan University, Wuhan, China; ^cNational Engineering Research Center of

Geographic Information System, China University of Geosciences, Wuhan, China; ^dCenter for Data Science, Peking University, Beijing, China;

^eSchool of Remote Sensing and Information Engineering, Wuhan University, Wuhan, China

ABSTRACT

Impervious surface has become one of the key factors of regional environmental problems and disasters. There rises an urgent need for mapping large-scale high-resolution impervious surfaces to help delicate modeling and overall planning. In the existing large-scale impervious surface mapping studies, there are many studies and products at medium resolution (10 ~ 100 m), some of which are with time series; while only few are at high resolution (<10 m), but not appeared with temporal updates. In the conventional scheme for large-scale high-resolution mapping, plenty of high-resolution imagery (HRI) are required to cover the entire large area and achieve wider coverage as much as possible. The high cost of obtaining abundant HRI limits large-scale high-resolution impervious surface mapping, leading to rare high-resolution impervious surface study at large scales. To alleviate the difficulties in the conventional scheme, an on-demand HRI scheme was proposed based on geospatial distribution knowledge (low overall proportion and high geospatial aggregation) of impervious surface at large scales, with the advantage of reducing the demand for HRI while ensuring coverage. Adopting the information and knowledge obtained from medium-resolution impervious surface data at large scales, the proposed on-demand HRI scheme only requires HRI where it is really needed, rather than for the entire large area as in the conventional scheme. Reducing the study area by a morphology-based method and selecting necessary HRI by the bidirectional image filtering (BIF) strategy, the on-demand HRI scheme has a smaller requirement of the HRI resources. The proposed on-demand HRI scheme and conventional scheme were implemented and discussed in five study areas. The results show that compared with the conventional method, the proposed on-demand HRI scheme reduced the requirement of HRI while ensuring coverage; and in the case of insufficient HRI coverage, it can reduce the HRI requirements while narrowing data gaps in the large-scale high-resolution impervious surface result. It was also found that the proposed scheme performs well in large-scale areas with low overall proportion and high geospatial aggregation of impervious surface found in the medium-resolution remote sensing product. Additionally, the on-demand HRI scheme will be also useful for large-scale high-resolution mapping of other land cover types.

ARTICLE HISTORY

Received 23 September 2020

Accepted 23 March 2021

KEYWORDS

Large-scale high-resolution mapping; medium-resolution; impervious surface; geospatial distribution knowledge; morphology-based; image filtering

1 Introduction

Impervious surface usually refers to the land surface covered by materials which prevent water infiltration into the deeper surface soil. From the perspective of urban geography, the distribution of impervious surface indicates regional prosperity. Monitoring impervious surface has attracted wide attention for urban studies. However, with the economic construction and expansion of the impervious surface, it becomes one of the key factors of urban environmental and ecological problems, such as urban heat island (Deng and Zhu 2020; Ziter et al. 2019), ecosystem services (Xu, Wang et al. 2018; Huang, Han et al. 2019),

emission and air pollution (Huang, Cai, and Li 2019; Khare et al. 2020). What's more, different from the natural surface, the emergence and rapid expansion of impervious surface accelerate surface runoff, reduce surface infiltration, weaken the duration of transpiration, and promotes the risk of urban flood and waterlogging disasters (Hung, James, and Hodgson 2018; Yu, Zhao, and Fu 2019; Baker, Schley, and Sexton 2019). Generally, those atmospheric, ecological, environmental problems and disasters do not appear independently in a small-scale area of a single city, but happen in a large-scale area consisting of multiple cities. It is difficult for a single city to take

care of itself. Large-scale overall planning is required to alleviate the problems and disasters. For example, the heavy rains and floods swept southern China in the summer, and the smog affected most of China in the winter. Therefore, there rises an urgent need for mapping large-scale high-resolution impervious surface, which is helpful for delicate modeling and overall planning.

There have been many studies and remotely sensed impervious surface products at medium or high resolution for large-scale analysis. At the global scale, there are several impervious surface related products, including: (1) HBASE in 2010, 30 m resolution (Wang et al. 2017); (2) GHS-BUILT in 2015, 30 m resolution (Corbane et al. 2019); (3) MSMT-2015, 30 m resolution (Zhang et al. 2020); (4) GlobeLand30 in 2000, 2010, 2020, 30 m resolution (Chen et al. 2015); (5) GlobeUrbanLand in 1980, 1990, 1995, 2000, 2005, 2010, 2015, 30 m resolution (Liu et al. 2018); (6) GAIA for every year from 1985 to 2018, 30 m resolution (Gong et al. 2020); (7) FROM-GLC10 in 2017, 10 m resolution (Gong et al. 2019). At the national scale, NLCD released 30 m impervious surface in the United States for 2001, 2006, 2011, and 2016 (Homer et al. 2020); (Kuang et al. 2020) developed 30 m annual impervious surface in China from 2000 to 2018; (Li et al. 2020) mapped 30 m China impervious surface in 2015; (Lin et al. 2020) produced annual 30 m China impervious surface from 2015 to 2018; (Shao et al. 2018) generated 2 m China impervious surface in 2017. At the urban agglomeration scale, (Zhang and Weng 2016) extracted annual 30 m impervious surface from 1988 to 2013 in Pearl River Delta, China; (Zhang, Zhang, and Yao 2018) developed seasonal impervious surface dynamics from 2000 to 2016 in Wuhan urban agglomeration, China; (Liu et al. 2020) mapped annual 30 m impervious surface from 1987 to 2017 in Middle Yangtze River Basin (MYRB), China; (Patidar and Keshari 2020) estimated annual 30 m impervious surface fraction from 1992 to 2017 in the National Capital Region, India. At the small scale as a single city or smaller, there are many methods and applications in mapping 10–30 meter level resolution impervious surface using Landsat, Sentinel, Hyperion, Gaofen 1, HuanJing 1 imagery (Shao et al. 2016; Tang and Hanqiu 2017; Xu, Liu, and Xu 2018; Bian et al. 2019; Misra, Kumar, and Shekhar 2020; Tang et al. 2020; Deng and Zhu 2020), and meter or sub-meter level high-resolution impervious surface based on

IKONOS, Quickbird, WorldView, ZiYuan-3, Gaofen 2 imagery (Lu and Weng 2009; Lu, Hetrick, and Moran 2011; Hu and Weng 2011; Cai, Li, and Jin 2016; Zhu et al. 2018; Zhang and Huang 2018; Dahiya, Garg, and Jat 2019; Yu et al. 2016; Feng and Fan 2019). The above-mentioned impervious surface studies can be analyzed in terms of resolution levels and compared from the perspective of spatial coverage and temporal update. According to the definition in resolution level of impervious surface (Weng 2012), high resolution refers to the spatial resolution less than 10 meter, while medium resolution indicates less than 100 meter. From the perspective of spatial coverage, those existing impervious surface studies can be divided into two types: large scale (global, national, or urban agglomeration) and small scale (single city or smaller). At large scales, there are many studies at 30 m resolution, only few at 2 m (Shao et al. 2018) or 10 m (Gong et al. 2019) resolution. At small scales, resolution level of impervious surface ranges from sub-meter, meter to tens of meters, and several related studies have been investigated for each level. From the perspective of temporal updates, there are several annual and few seasonal updated impervious surface mapping studies at medium resolution. In summary, there are many studies on large-scale medium-resolution impervious surface, part of which are time-series; while large-scale high-resolution study is rare and not appeared with temporal updates.

The reason for rate high-resolution impervious surface study at large scales is the difficulty in obtaining abundant high-resolution imagery (HRI) resources. HRI is the only type of imagery that can generate high-resolution impervious surface products. In the conventional scheme for large-scale high-resolution mapping, hundreds, thousands, or even more HRI are required to cover the entire large area and achieve wider coverage as much as possible. Thus, the conventional scheme is also called the full HRI scheme in this paper. However, HRI is almost always used for commercial purposes. The high cost of acquiring enough HRI is the primary factor hindering high-resolution impervious surface mapping at large scales (Wang and Li 2019). Moreover, affected by atmospheric conditions and satellite revisiting period, the satellite data gaps are another hinder for large-scale high-resolution impervious surface mapping. The conventional full HRI scheme for large-scale high-

resolution impervious surface mapping is highly resource-intensive, and gaps may exist in the high-resolution impervious surface result.

The studies on the large-scale land surface mapping are investigating toward higher resolution (Feng and Xin 2020). The technology on large-scale impervious surface mapping has gradually matured at medium resolution, and many products appeared with high performance. The rich information in large-scale medium-resolution impervious surface products could provide support for mapping high-resolution impervious surface at large scales. This study hopes to use the information and knowledge found in medium-resolution impervious surface data to alleviate the difficulties in the conventional full HRI scheme, and improve the efficiency of mapping high-resolution impervious surface at large scales. The goal of this study is to explore the geospatial distribution characteristics and knowledge of impervious surface at large scales from medium-resolution impervious surface data, then use it to select HRI where it is really needed, reducing the demand for HRI while ensuring the spatial coverage in mapping high-resolution impervious surface at large scales. There are two questions to be solved in this study:

- (1) How to explore the geospatial distribution characteristics and knowledge of impervious surface at large scales from medium-resolution remote sensing product.
- (2) How to find the places where HRI is really needed and select HRI on demand under the guidance of the geospatial distribution knowledge above, with the advantage of reducing the demand for HRI while ensuring coverage in mapping large-scale high-resolution impervious surface.

2 Study area and materials

Middle Yangtze River Basin (MYRB) urban agglomeration is the first approved national urban agglomeration and important part of The Belt and Road. Located in central China, MYRB urban agglomeration consists of 3 megacities and 28 large or medium-sized cities. Covering an area of 326,000 km² across Hubei, Hunan, and Jiangxi province, MYRB is the second largest urban agglomeration among 5 national urban agglomerations approved by the Chinese government until the end of 2019. From the 2017 national statistics, MYRB has created 9.6% of the

total economic output with 3.4% of the land area and 9.0% of the population.

Wuhan Megalopolis (WM), Changsha-Zhuzhou-Xiangtan Megalopolis (CZTM), and Poyang Lake Megalopolis (PLM) are regional megalopolises located in MYRB, gathering the main economies, populations, technology, education, transportation, and other resources of Hubei, Hunan, and Jiangxi provinces, respectively. Each megalopolis contains a megacity and several cities with strong connections around it. More specifically, WM consists of Wuhan and 8 surrounding cities (Huangshi, Ezhou, Huanggang, Xiaogan, Xianning, Xiantao, Qianjiang, and Tianmen) accounting for 58,000 km², CZTM containing Changsha and 2 surrounding cities (Zhuzhou and Xiangtan) with 28,000 km², PLM including Nanchang and 5 surrounding cities (Jiujiang, Shangrao, Yingtan, Jingdezhen, and Fuzhou) with 77,000 km². Besides, Wuhan (WH) is the only national central city and the most prosperous big city in central China. Covering about 8,600 km², WH is an important industrial, science and education base, and comprehensive transportation hub in the national perspective, with the goal of driving and realizing the rise of the central China region. Shown as (Figure 1), the study areas include three scales: (1) large scale, national urban agglomeration composed of several megacities and dozens of cities, taking MYRB as a use case; (2) medium large scale, regional megalopolis containing one megacity and several cities, with WM, PLM, and CZTM as use cases; (3) small scale, a single city, as a compared scale to analyze the applicability of the proposed scheme, taking WH as a use case.

Remotely sensed impervious surface product and government statistics are utilized to explore the geospatial distribution characteristics of impervious surface at large scales. GAIA is an annual 30-meter remotely sensed impervious surface product based on Landsat satellite imagery from 1985 to 2018 (Gong et al. 2020). With the long time series and full spatial coverage, GAIA is also adopted as the medium-resolution impervious surface in the steps of the proposed scheme. Government statistics are collected from the 2018 statistical yearbook of urban construction published in 2020 by the Ministry of Housing and Urban-Rural Development of the People's Republic of China (<http://www.mohurd.gov.cn/xytj/tzlsxtjgb/jstnjn/>).

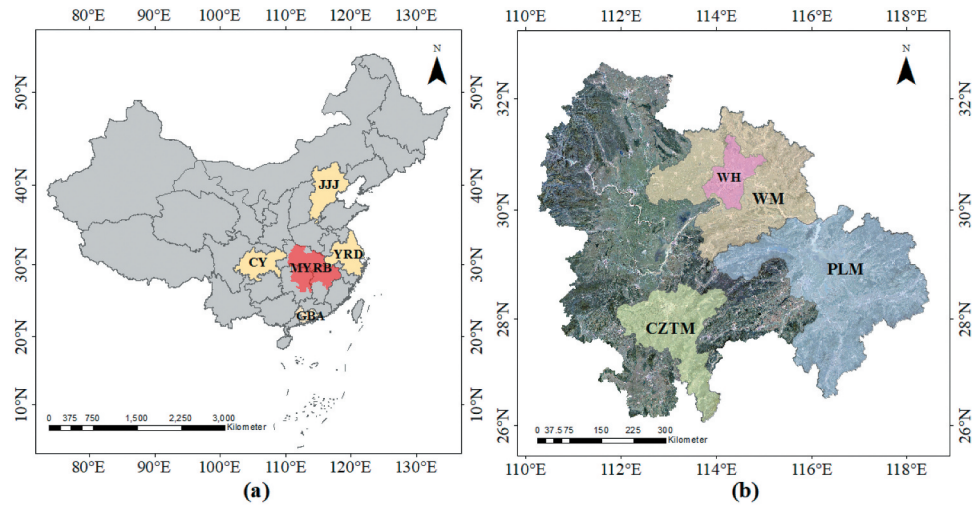


Figure 1. The location of the study areas: (a) five national urban agglomerations in China (JJJ: Jing-Jin-Ji, YRD: Yangtze River Delta, CY: Cheng-Yu, GBA: Guangdong-Hong Kong-Macao Greater Bay Area) (b) five study areas in three scales, where MYRB is one of five national urban agglomerations as large scale, WM, PLM and CZTM are three regional megalopolises as medium-large scale, WH is a prosperous single city as small scale.

Gaofen 2 imagery is employed as the HRI data source in this study. Equipped with a 0.8-meter panchromatic and 3.2-meter 4-band multispectral sensor, Gaofen 2 is one of several sub-meter level high-resolution remote sensing data sources. Since Gaofen 2 is an optical remote sensing data, cloud cover is one of the main factors affecting the image quality. Image data with cloudiness within 10% is selected as the high-quality image (Meraner et al. 2020). Gaofen 2 images were obtained from China Center for Resources Satellite Data and Application, and Hubei High Resolution Satellite Application Center. To match the available time, Gaofen 2 and GAIA were collected from 2016 to 2018. The available Gaofen 2 image resources with cloudiness within 10% for each study area are listed in (Table 1), which will be regarded as the original HRI dataset in this study.

3 Geospatial distribution characteristics of impervious surface at large scales

The geospatial distribution characteristics of impervious surface at large scales would be quantitatively explored from the two perspectives: one is to analyze the overall proportion of impervious surface (PIS) in the entire area from a global perspective; the other is to explore the geospatial aggregation phenomenon of the impervious surface with the surroundings from a local perspective. However, different from describing the phenomenon of landscape aggregation by agglomeration index in

Table 1. Available Gaofen 2 image resources of five study areas in three scales.

Scales	Regions	Years	Scenes ^a	Coverage rates ^b (%)
National urban agglomeration	MYRB	2016	1431	87.14
		2017	1358	84.98
Regional megalopolis	PLM	2018	1395	79.27
		2016	281	86.27
		2017	230	71.94
		2018	210	58.65
		2016	177	95.47
CZTM	CZTM	2017	132	91.26
		2018	147	79.85
		2016	477	95.94
		2017	304	86.84
		2018	374	96.52
WM	WM	2016	169	100
		2017	33	66.26
		2018	85	99.56
City	WH	2016	169	100
		2017	33	66.26
		2018	85	99.56

^aOnly high-quality images with cloudiness within 10% are collected as available Gaofen 2 images, which will be regarded as the original HRI dataset in this study.

^bCoverage rate refers to the mosaic coverage of all available Gaofen 2 images divided by the corresponding total study area.

landscape analysis (Schumaker 1996; Li and Wu 2004), the land surface geospatial aggregation analysis in this study is to measure the local geospatial similarity of each land surface location with the surroundings, and thereby explore the geospatial aggregation effect of impervious surface at large scales. So, a harmonized geospatial aggregation distribution index (HGADI) was proposed to describe the geospatial aggregation degree based on remotely sensed impervious surface product.

3.1 Overall proportion

With high overall accuracy and time series, the remotely sensed impervious surface product can capture the overall proportion of impervious surface at large scales. Based on Eq. (1), it can make statistics on the PIS for any observable spatiotemporal range. Utilizing GAIA to depict the impervious surface in long time series, the PIS in five study areas were calculated from 1985 to 2018, shown as (Figure 2). It is easy to find that the PIS is increasing year by year, and the maximum value appears in the year closest to the present. PIS in large-scale areas are at a low level (<10%) in the recent decades, where MYRB, PLM, and CZTM having PIS with a very low level (<5%). However, PIS in the city scale is much higher than in the large scales. A conclusion could be drawn from remotely sensed impervious surface product as that the PIS in large-scale areas are very low from past to now and highly likely to continue to be at a low level in the foreseeable future.

$$PIS = \frac{A_{IS}}{A_{total}} \times 100\% \quad (1)$$

A_{total} means the total area of the region. A_{IS} refers to the total area of the impervious surfaces.

Due to the inevitable errors in remote sensing products, government statistics are good supplementary supporting information. As the definition of buildup district in the statistical yearbook is the most similar to urban impervious surface in statistical

material, the PIS can also be calculated from government statistics. According to the 2018 statistical yearbook of urban construction published in 2020, the total national area of the buildup district is 58,456 km². Due to a vast territory and significant geographical differences, compared to the national land area of 9,600,000 km², PIS is only 0.61% in 2018. Even this seemingly low PIS in 2018 is the great achievement from urban expansion brought about by the rapid development of China's reform and opening up. (Figure 3) shows the PIS for 28 large-scale province-level regions in China mainland calculated from the 2018 statistical yearbook. Almost all provinces have a very low PIS value less than 5%, where higher PIS would appear in the areas with higher level of economic development. There are 16 provinces with PIS less than 1%, 8 provinces with PIS in 1–2%, 1 province (Zhejiang) with PIS in 2–3%, 2 provinces (Guangdong and Shandong) with PIS in 3–4%, and 1 province (Jiangsu) with PIS in 4–5%. Absolute values of PIS are at very low level from the statistical data, which again confirms the conclusion from the remotely sensed data.

3.2 Geospatial aggregation phenomenon

Calculating regional PIS is a straightforward way to express the overall distribution of impervious surface from the global perspective, but it is impossible to represent the distribution characteristics from a local perspective. In Tobler's First Law of Geography, a land surface target has a higher relationship and similarity

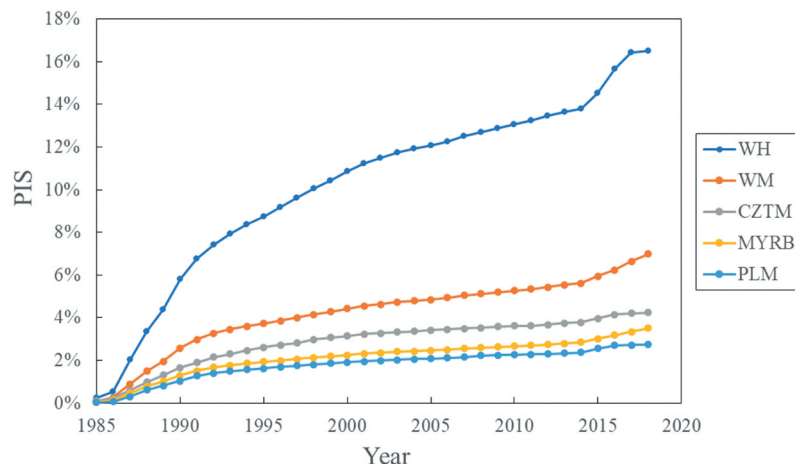


Figure 2. The proportion of impervious surface (PIS) in five study areas from 1985 to 2018 based on medium-resolution impervious surface product (GAIA).

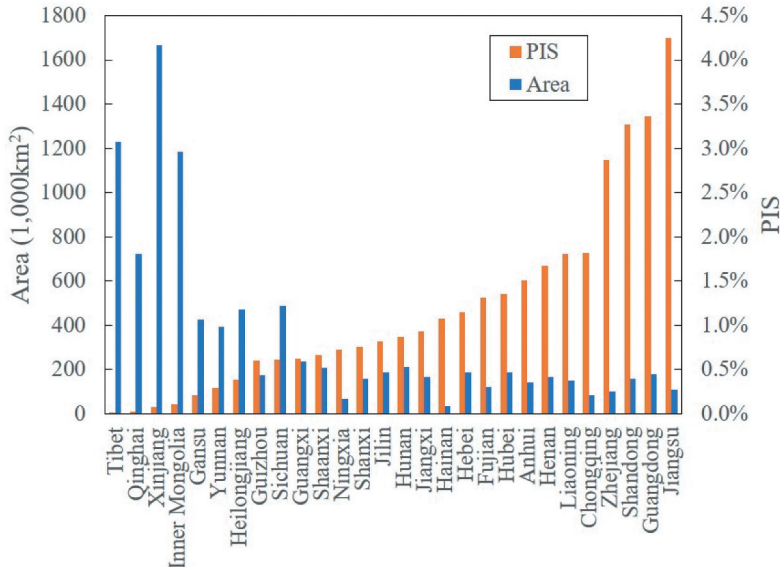


Figure 3. The PIS of 28 province-level regions in China mainland based on government statistics in 2018.

with surfaces nearby than distant (Tobler 1970), which can explain the geospatial aggregation distribution of the impervious surface particularly noticeable in the main urban area. A geospatial aggregation distribution index (GADI) was proposed to characterize the geospatial aggregation phenomenon of a certain land surface type by using the statistic of the neighborhoods' similarity, formula shown as Eq. (2). In measuring the local similarity, an issue that needs to be determined manually is that how many neighbors at each location should participate in the neighborhood similarity calculation. 8-neighborhood was adopted in this study. The neighborhood similarity for each center location ranges from 0 to 1. When 4 neighbors are the same land surface type as the central location, the local similarity of this location would be 0.5. GADI can indicate the geospatial aggregation distribution degree for one kind of land surface type.

To characterize the geospatial aggregation in a comprehensive way, the harmonized GADI (HGADI) was designed where geospatial aggregation characteristic of each surface type is taken into consideration, as shown in the formula as Eq. (3). In a binary classification system, such as impervious surface mapping, not only the target (impervious surface) is of high importance, but also the background (pervious surface) which could describe the geospatial aggregation of the target surface from the opposite perspective. In the impervious surface study, the formula of HGADI was specific as Eq.

(4) from Eq. (3), and HGADI is ranged in (0.5, 1), when the target and the background obey the chessboard distribution, HGADI will usher in the minimum value equaling to 0.5. The closer HGADI is to 1, the higher degree of geospatial aggregation.

$$GADI_i = \frac{\sum_{j=1}^{m_i} p_{ij}}{m_i} \quad (2)$$

$GADI_i$ means the GADI of the i -th land surface type. p_{ij} is the neighborhood similarity of j -th location or pixel in the i -th land surface type. m_i is the amount of the total targets or pixels of the i -th land surface type in the entire study area.

$$HGADI = \sum_{i=1}^n P_i \times GADI_i \quad (3)$$

P_i is the proportion of the i -th land surface type in the entire area. n is the amount of land surface types.

$$HGADI_{IS} = P_{IS} \times GADI_{IS} + P_{PS} \times GADI_{PS} \quad (4)$$

$$P_{PS} = 1 - P_{IS} \quad (5)$$

$HGADI_{IS}$ refers to HGADI in impervious/pervious surface classification system, which will be shown as HGADI in the later part of this paper. P_{IS} is the proportion of impervious surface, as PIS in Eq. (2). P_{PS} is the proportion of pervious surface.

Using GAIA data in 2018, geospatial aggregation distribution characteristics were generated for five

Table 2. Geospatial aggregation distribution index calculation results of five study areas in three scales.

Scales	Regions	Indicators	Land surface types		
			IS	PS	HGADI
National urban agglomeration	MYRB	P_i	3.51%	96.49%	0.9818
		$GADI_i$	0.7401	0.9905	
Regional megalopolis	PLM	P_i	2.74%	97.26%	0.9858
		$GADI_i$	0.7406	0.9927	
	CZTM	P_i	4.23%	95.77%	0.9848
		$GADI_i$	0.8207	0.9921	
City	WM	P_i	6.98%	93.02%	0.9618
		$GADI_i$	0.7266	0.9795	
City	WH	P_i	16.50%	83.50%	0.9285
		$GADI_i$	0.7833	0.9572	

IS refers to impervious surface, PS refers to pervious surface.

study areas in three scales. As shown in (Table 2), the HGADI results of five regions are more than 0.9, implying the degree of geospatial aggregation distribution. In the large scales including national urban agglomeration and regional megalopolis, the PIS are less than 10% and HGADI more than 0.95. Especially, MYRB, PLM, and CZTM have PIS of less than 5% and extremely high HGADI of more than 0.98. However, at the city scale, WH has a high PIS equaling 16.5% and relatively low HGADI equaling 0.9285. It can be easily deduced that large urban areas have a geospatial aggregation phenomenon, where more significant geospatial aggregation appears in larger scale areas. Furthermore, under the urban expansion phenomenon and time filtering rule which is often adopted in generating impervious surface product with long time series (Gong et al. 2020; Liu et al. 2020), the impervious surface result of the next year would increase on the basis of the previous year, it can be further inferred that there is still a high geospatial aggregation distribution for the impervious surface at large scales for a long period.

4 On-demand HRI scheme for large-scale impervious surface mapping

4.1 Architecture of the on-demand HRI scheme

From Section 3, there finds the knowledge of low overall proportion and high geospatial aggregation in impervious surface at large scales. That means most of the land surfaces are covered by pervious surface with noticeable geospatial aggregation, where it is unnecessary to use HRI for impervious surface mapping. The reality and knowledge above triggered the

on-demand HRI scheme proposed in this study to generate large-scale high-resolution impervious surface using a smaller amount of HRI. The key point of impervious surface mapping should be the impervious surface rather than pervious surface. Regardless of the resolution of the remote sensing data source, there should be no difference in impervious surface mapping result for typical pervious surface areas, such as forest and lake. Medium-resolution imagery (MRI) is sufficient in those places, HRI is not necessary. However, for impervious surface and areas nearby, there comes a real need for HRI to delineate impervious surface at high resolution. With the knowledge of low overall proportion and high geospatial aggregation and the help of medium-resolution impervious surface data, fewer HRI are required in the proposed on-demand HRI scheme for those regions containing impervious surfaces, rather than the total area. The idea of the proposed on-demand HRI scheme and conventional full HRI scheme are compared in the conceptual schematic diagram shown in (Figure 4).

Based on the idea and knowledge above, the architecture of the on-demand HRI scheme was designed for mapping large-scale high-resolution impervious surface. Shown as (Figure 5), it consists of three main steps: 1. medium-resolution impervious surface preparation, 2. unnecessary HRI reduction, and 3. high-resolution impervious surface generation. The first is to prepare the medium-resolution impervious surface for the total study area. Medium-resolution impervious surface result would be generated from MRI. Then, it comes the key part of the proposed on-demand HRI scheme. In Step2 unnecessary HRI reduction, a morphology-based method was applied to find large continuous pervious surfaces and reduce target study area from the medium-resolution impervious surface data. For the reduced study area, only necessary HRI would be selected by a proposed bidirectional image filtering (BIF) strategy. Finally, high-resolution impervious surfaces are generated from HRI in the reduced study area. After extracting impervious surface from HRI scene by scene, high-resolution impervious surface results in the total study area would be generated by mosaicking the result of each scene HRI and the pervious surfaces recognized in Step2.

In the architecture of the on-demand HRI scheme, Step1 and Step3 are usual processing in the

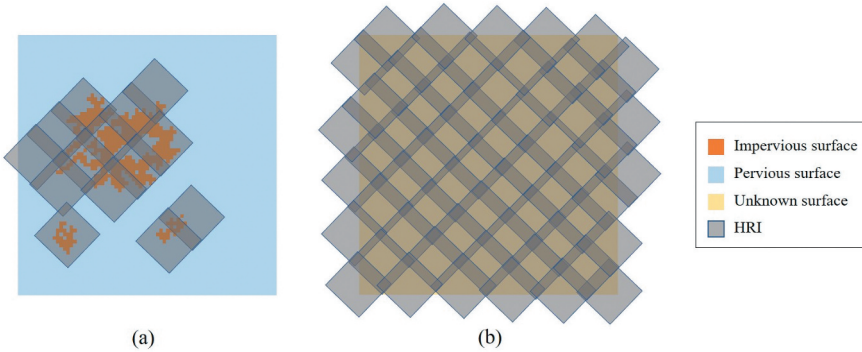


Figure 4. The diagram of the main idea: (a) proposed on-demand HRI scheme based on medium-resolution impervious surface data, where fewer HRI are required in the regions containing impervious surfaces, rather than the total area (b) conventional full HRI scheme, where the entire study area are unknown surfaces and need large amount of HRI to achieve full coverage.

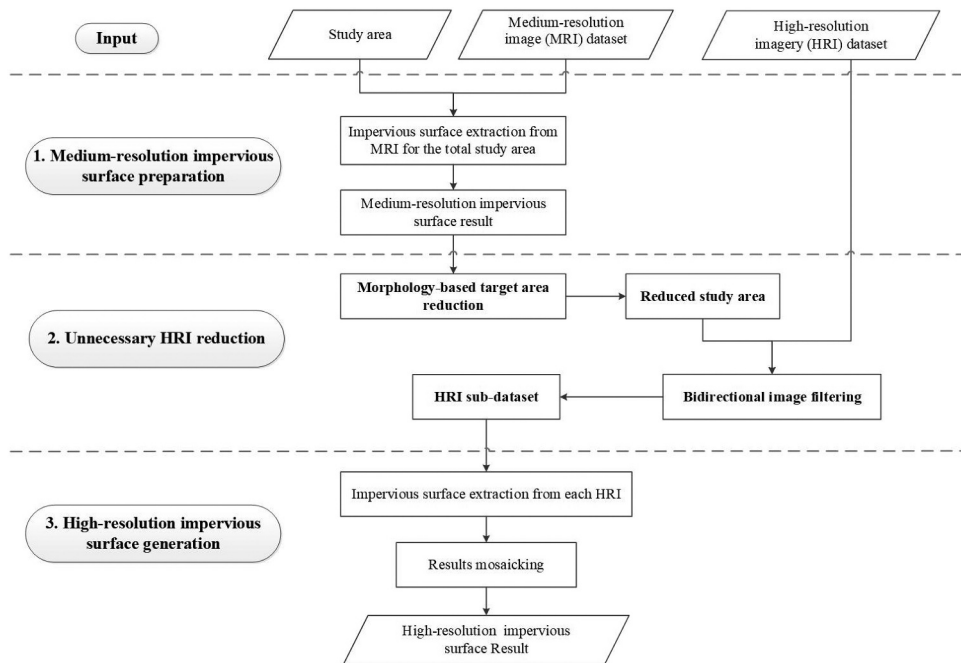


Figure 5. The workflow of the on-demand HRI scheme for mapping high-resolution impervious surface at large scales.

conventional impervious surface mapping application, where the main process is to extract impervious surface from remote sensing image by a powerful classification algorithm, such as random forest, support vector machines and object-based method (Mountrakis, Im, and Ogole 2011; Sugg et al. 2014; Xu, Mountrakis, and Quackenbush 2017; Bramhe, Ghosh, and Garg 2019). Step1 is utilized for MRI, Step3 for HRI. If there is an available medium-resolution impervious surface product with good quality, such as GAIA, it can be utilized directly to finish Step1 medium-resolution impervious surface preparation.

As the core part of the proposed on-demand HRI scheme, Step 2 is to reduce the demand for HRI while

ensuring coverage, and thereby improve the efficiency in large-scale high-resolution impervious surface mapping. As masking pervious surfaces is an effective approach for mapping impervious surface (Huang et al. 2018), large continuous pervious surfaces can be removed from the total study area. After removing most of the obvious pervious surface, the study area would be smaller, thereby it can reduce the demand for HRI data and calculation resources. There are two key issues in Step2 unnecessary HRI reduction: one is how to reduce the target area, the other is how to select those necessary HRI. By preserving the impervious surfaces in Step1's result and expanding them several times to cover neighboring areas, the morphology-

based method could reduce the target area, suppress the influence of the inevitable errors in the impervious surface generated from MRI, and thereby increase the reliability and performance in the following steps. Using two modes of image filtering, a proposed BIF strategy could select necessary HRI in the reduced target area, achieving the highest coverage of HRI dataset and lowest HRI requirement at the same time.

4.2 Morphology-based target study area reduction

In the proposed scheme for large-scale high-resolution impervious surface mapping, HRI is not necessary for the total area, especially those areas covered by large pervious surfaces, such as forests and lakes. The study area can be reduced by removing large pervious surfaces and using the medium-resolution results from Step 1. Once the study area is reduced, the amount of required HRI will also decrease. For the study area reduced method, there are several special requirements in the proposed scheme to guarantee the performance of the following steps for high-resolution impervious surface generation: (1) preserve impervious surfaces in Step1's result; (2) enlarge those impervious surfaces to cover the area nearby, which has a high potential for existing some impervious surfaces that cannot be recognized by MRI due to pixel confusion but can be identified by HRI, and thereby improve the performance of Step3; (3) remove the obvious pervious surfaces, such as river, lake, and forest; (4) make the boundary of the reduced target study area as simple and smooth as possible, to reduce the complexity and time consumption in the following step of HRI filtering.

Morphology transformation is an effective method to enhance the effect of the remote sensing results by the removal of unnecessary morphological features (Benediktsson, Pesaresi, and Arnason 2003; Chen, Trinder, and Niu 2017; Zhang and Huang 2018). Erosion and dilation are the most common and basic morphology operations, based on which several advanced and complex operations can be combined, such as opening, closing, morphological gradient, top hat, and black hat. To meet four special requirements of target study area reduction, a morphology-based method was designed with two rounds of morphological closing operation. The closing operation is a dilation operation followed by an erosion operation, which is powerful for closing small holes and dots in target objects, and protecting the large and prominent background objects at the same time. The reason for two rounds of closing operation is because the second round has to deal with small holes and fragments in the result of the first round. Besides, the size of the kernel in the morphological operator is a vital parameter to be adjusted. After adjusted kernel size manually many times in the study areas, the size of 33×33 is adopted in this study. In the 30 m resolution impervious surface result of Step1, the kernel of 33×33 refers to a 990 m \times 990 m window, whose performance is similar to 1 km level upscaling resampling in some way. The difference from upscaling resampling is that this morphology-based method protects obvious pervious surfaces. (Figure 6) shows the performance of the morphology-based method for reduced target area generation in a typical region, where the central ribbon area is the Yangtze River in this region. Small pervious surfaces were occupied, but main surfaces were protected. After vectorization,

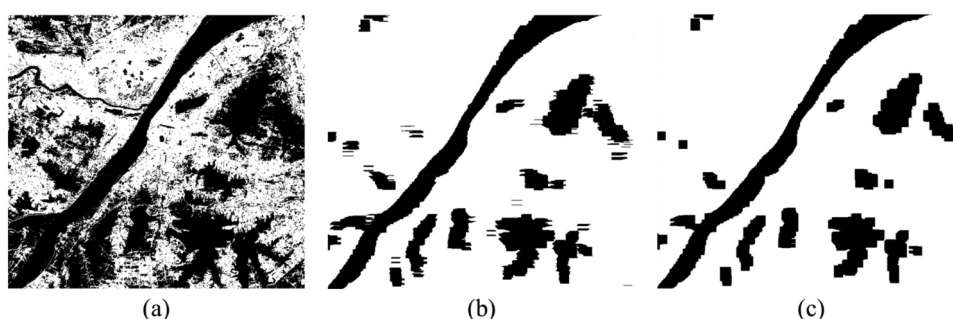


Figure 6. The performance of the morphology-based method for reduced target area generation: (a) medium-resolution impervious surfaces, (b) first round of closing operation, (c) second round of closing operation. Color in white and black are the impervious and pervious surfaces, respectively.

the boundary of the reduced target area would be created for the following step of HRI filtering in this scheme. As the size of the target study area is reduced and becomes smaller than the total study area, there will come a smaller requirement for HRI which is only necessary to cover the reduced study area.

4.3 Bidirectional image filtering strategy

For large-scale mapping, a large amount of image resources is required. There comes a need to select the necessary image from the dataset. As the coverage of HRI is too small when compared to large-scale areas, it would adopt hundreds or thousands of images to achieve the highest coverage of the total area. What's more, due to the irregular revisit coverage of the HRI, such as Gaofen 2, it cannot filter images in an easy way as the regular observation code (path and row number) as Landsat. There requires a detailed coverage boundary for each observation to find enough images to cover the total large study area. A BIF strategy was employed to select necessary HRI data to achieve the highest coverage of the HRI dataset and lowest HRI requirement for the target area.

The BIF strategy consists of two main parts, expansion filtering mode and reduced filtering mode. Firstly, the expansion filtering mode goes through all available images and calculates the corresponding coverage rate of the target area, picks the images with high coverage rate one by one from inside to outside, to ensure the highest coverage as possible as the image data source can. The output image dataset of expansion filtering mode is a sufficient sub-dataset of the original image dataset to realize the highest coverage of the target area, but may exist some places were re-covered by multiple images. Then, the reduced filtering mode gets up on stage. It checks the necessity of each image in the result image dataset of expansion filtering mode. If an image was removed from the dataset, the coverage of the remaining image dataset for the target area was still the same, then this image will be picked out. After the reduced filtering mode, the final sub-dataset not only reaches the highest coverage in the study area, but also improves the efficiency of image use.

The detailed steps in BIF are shown as below:

Input: target area ($A_{target_initial}$), image dataset ($D_{initial}$)

1: Update the target area with a total coverage capability of $D_{initial}$.

Calculate the largest coverage ($A_{initial_images}$) of the $D_{initial}$ in $A_{target_initial}$ by merging all images in $D_{initial}$ and intersecting with $A_{target_initial}$.

$$A_{target} = A_{initial_images} \cap A_{target_initial}$$

2: Pick up images from $D_{initial}$ by expansion filtering mode.

(i) Initialize the input target area of this step.

$$A_{target_expan} = A_{target}$$

(i) Calculate the coverage rate in A_{target_expan} for each image in $D_{initial}$.

(ii) Sort all images in $D_{initial}$ by coverage rate, pick up one image with the highest coverage rate into the result image dataset of expansion filtering mode (D_{expan_mode}), update $D_{initial}$ by picking out this selected image.

(iii) Re-update the target area. Calculate the largest coverage (A_{expan_mode}) of the D_{expan_mode} in A_{target} , update target area by erasing A_{expan_mode} .

$$A_{target_expan} = A_{target} - A_{expan_mode}$$

(i) Repeat steps 2. ii.-iv., until the $A_{target_expan} = null$.

3: Pick out the unnecessary images from D_{expan_mode} by reduced filtering mode.

(i) Initialize the input image dataset of this step.

$$D_{reduce_mode} = D_{expan_mode}$$

(i) Go through all images in D_{expan_mode} from the first one to the last one, check the corresponding necessity. When an image is picked out, a new temporary image dataset (D_{reduce_temp}) would be created by the remaining images in D_{expan_mode} . Calculate the total coverage (A_{reduce_temp}) of the D_{reduce_temp} in A_{target} . If $A_{reduce_temp} \cap A_{target} == A_{target}$, then the image is indeed unnecessary and should be picked out, $D_{reduce_mode} = D_{reduce_temp}$, at the same time, stop this round of traversal, and restart a new round of Step3.ii.

(ii) Final output image dataset $D_{final} = D_{reduce_mode}$.

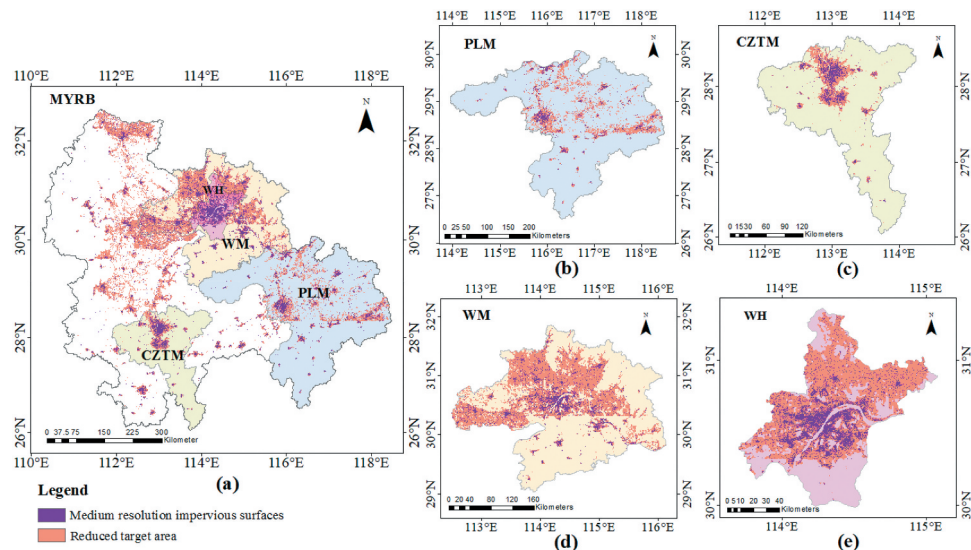


Figure 7. Target area reduced effect of the proposed scheme in five study areas.

5 Results and discussion

According to the scheme and methods in Sections 3 and 4, experiments were implemented in five study areas of three scales in Section 2 for each year from 2016 to 2018. GAIA was regarded as the medium-resolution impervious surface result of Step1. For geospatial distribution analysis of large-scale impervious surface, the PIS and HGADI were calculated using the Environment for Visualizing Images (ENVI) and Pixel Information Expert (PIE) software. Morphology-based reduced target area generation was conducted by ENVI. BIF strategy was developed as a C# program developed based on ArcEngine. As object-oriented classification is a powerful and widely used method for high-resolution land cover land use mapping based on HRI (Weng 2012; Sugg et al. 2014; Xu and Wang 2016; Feng and Fan 2019), the high-resolution impervious surface was extracted by Ecognition in Step3. All maps were generated by ArcMap. The conventional scheme requires large amounts of HRI data to cover the total study area, where large-scale high-resolution impervious surface results were generated by mosaicking the result of each scene of image in the required HRI dataset. The performance of the proposed on-demand HRI scheme and conventional full HRI scheme would be evaluated for five study areas in three scales and three years.

5.1 Target study area reduced effect of the on-demand scheme

Based on the geospatial distribution knowledge of impervious surface at large scales, the first key point in the on-demand HRI scheme is to reduce the target area based on medium-resolution impervious surface data. After removing large obvious background surfaces, a smaller target study area requires a smaller amount of the HRI resources. However, there exist inevitable errors in medium-resolution remotely sensed impervious surface data, especially for the boundary and edge areas. So simple method as vectorization of the medium-resolution impervious surface is not suitable for the transferred errors in the subsequent steps for mapping high-resolution impervious surface. Not only the impervious surfaces in Step1's result but also those areas nearby should be contained in the reduced target area, to prevent adverse effects and accumulative errors. Under the two rounds of morphological closing operation, the morphology-based method was implemented in five study areas, results shown as (Figure 7). From the visual comparison, the reduced target study areas are smaller than the corresponding total study areas, but larger than the area of impervious surfaces in GAIA.

To quantitatively evaluate the target area reduced effect, there utilized two indicators to assess the expansion rate on the impervious surfaces in GAIA, and the reduction rate on the total study area. (Table

Table 3. Target study area reduced effect of the proposed scheme.

Scales	Regions	Areas (km ²)	Expansion rates on GAIA's result	Reduction rates on total study area
National urban agglomeration	MYRB	326,000	398.23%	82.51%
Regional megalopolis	PLM	77,000	373.69%	87.04%
	CZTM	28,000	193.94%	87.56%
	WM	58,000	442.46%	62.13%
City	WH	8,600	296.82%	34.52%

3) shows the quantitative comparison and evaluation result of five study areas in three scales. For all three scales, the reduced target areas had expanded 193.94% to 398.23% of the impervious surfaces in GAIA, and reduced 34.52 to 87.56% of the total study area. About 2 to 4 expanded times of the suspected impervious surfaces brought great confidence to the next step of high-resolution impervious surface extraction. However, the reduction rate shows huge divergence at different scales where geospatial distribution characteristics of impervious surface are different. The reduction rates at large scales including urban agglomeration and regional megalopolis are much higher than at a small scale as a single city. For MYRB, the target area reduced effect is significant, with a reduction rate equaling 82.51%. The reduction rate of WH is only 34.52%. Low overall proportion and high geospatial aggregation in medium-resolution impervious surface data would guarantee high performance in target study area reduction. The level of the reduction rate directly determines the effect of the HRI demand reduction rate, implying that the better performance of the proposed on-demand HRI scheme will lie in large-scale areas.

5.2 Performance comparison and discussion in HRI requirement and coverage

To compare the performance equally, the HRI needed were selected by BIF strategy in both proposed on-demand HRI scheme and conventional full HRI scheme. Different from the full HRI scheme covering the total study area, the on-demand HRI scheme only requires the necessary HRI to cover the reduced study area in [Section 5.1](#). The conventional full HRI scheme and the proposed on-demand HRI scheme were implemented in five study areas of three scales and

three years, results shown as ([Figure 8](#)). It can be easily seen by visual comparison that the HRI requirement of the full HRI scheme, as shown in 2016 (I), 2017 (I), and 2018 (I), is more than the on-demand HRI scheme, as shown in 2016 (II), 2017 (II), and 2018 (II). To describe the performance in HRI requirement and coverage, several statistics were selected and calculated. Based on the results of 2016 (I), 2017 (I), and 2018 (I) in ([Figure 8](#)), three statistics were calculated for the conventional scheme, including required HRI amount, HRI required rate on original HRI dataset, and coverage rate on the total study area, results shown as ([Table 4](#)). Derived from results of 2016 (II), 2017 (II), and 2018 (II) in ([Figure 8](#)), the same three statistical indicators were generated in the same way for the on-demand HRI scheme, results shown as ([Table 5](#)). Furthermore, to compare the conventional and proposed scheme, ([Table 6](#)) was produced from ([Tables 4 and 5](#)) with five statistical indicators in absolute and relative differences.

In the full HRI scheme, compared with the original HRI dataset as ([Table 1](#)), ([Table 4](#)) shows the high performance of the BIF strategy in necessary HRI selection. With the same coverage of the original HRI dataset, BIF reduced a large amount of HRI from the original dataset for the total study area, which ushered in the highlight moment of BIF. At the largest scale, MYRB required 783–853 scenes of HRI from 2016 to 2018, with a reduced HRI required rate of more than 40%. At the regional megalopolis scale, it needs one to two hundred scenes of HRI to achieve its highest coverage of the original dataset. BIF employed 172–226 scenes and reduced about 30% HRI resources on the original dataset for PLM, applied 88–101 scenes of HRI, and lowered about 40% HRI resources for CZTM, utilized 167–196 scenes of HRI and decreased about 50% HRI resources for WM. At the small scale as a comparison, due to the large inter-annual change in the amount of available HRI resources, there are 33–169 scenes of HRI in the original HRI dataset. The effect of BIF in WH had a large degree of change, HRI required rate ranging from 24.26% to 69.70%, annual average of the reduced rate about 50%. In a summary, the BIF could guarantee to maintain the coverage of the original HRI dataset and reduce 30–50% HRI requirement in an average level, where the performance of the specific region will vary with the original HRI dataset of the corresponding spatial and temporal instance. On the

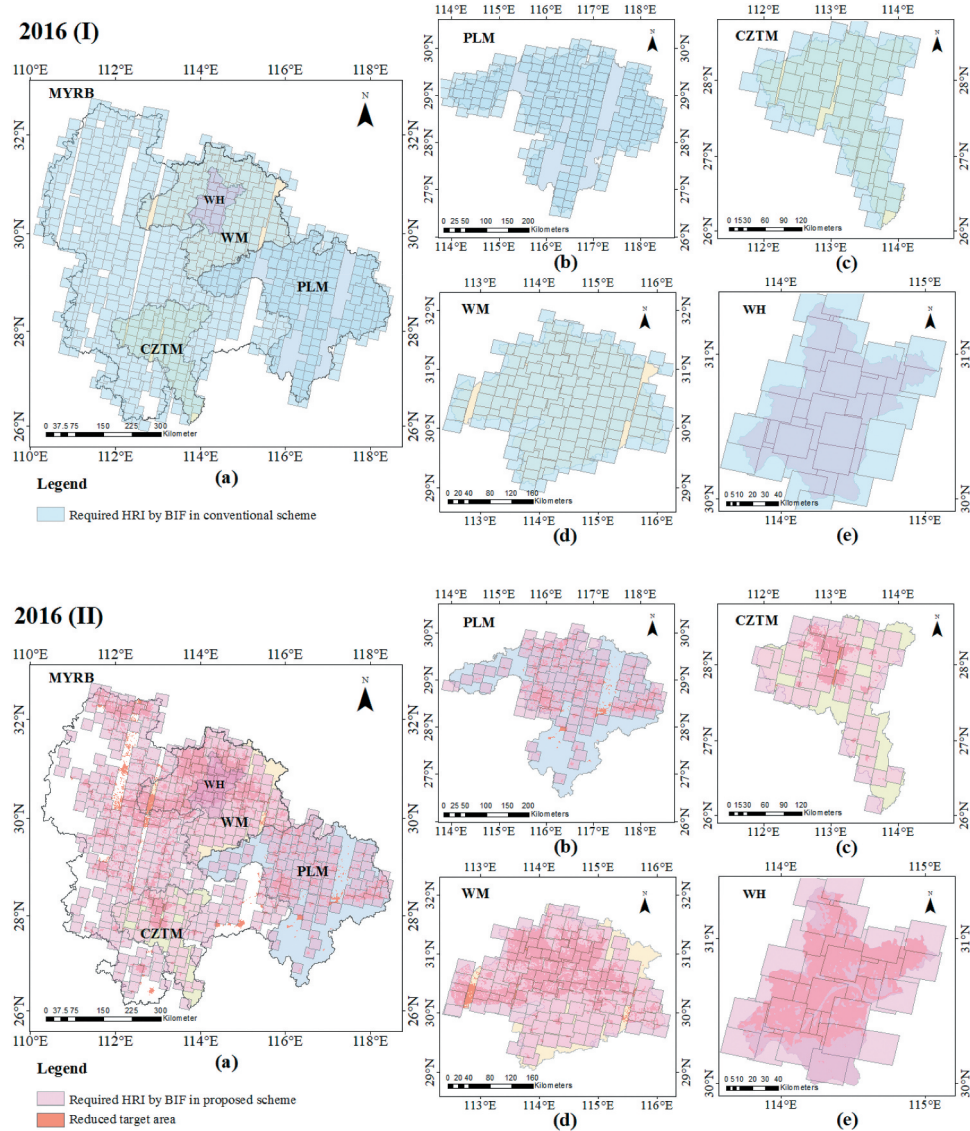


Figure 8a. HRI requirements in five study areas from 2016 to 2018: (I) the conventional full HRI scheme, (II) the proposed on-demand HRI scheme.

other hand, it is worth attention that the coverage rate on the total study area in the conventional full HRI scheme is not very high. Regarding one study area in a year as a case, there are 15 cases in five study areas and three years in this study. Only 6 in 15 cases (highlighted in Table 4) reached 90% coverage rate in the total study area. Most cases had coverage about 70% to 90%, whereas two extremely low coverage appeared in PLM 2018 with coverage of 58.65%, and WH 2017 with coverage of 66.26%. The data gaps that cannot be covered by usable HRI is a fatal problem in conventional full HRI scheme for large-scale high-resolution impervious surface mapping.

To evaluate the performance of the proposed on-demand HRI scheme, the same three indicators as the conventional scheme in (Table 4) were generated in the same way, results shown as (Table 5). Under the BIF strategy for the reduced target areas, the necessary HRI were further decreased for all five regions and three years. In the on-demand HRI scheme from 2016 to 2018, MYRB need 544–609 scenes of HRI, PLM required 99–139 scenes, CZTM employed 47–56 scenes, WM utilized 130–153 scenes, WH used 22–37 scenes, with about 60% reduction on original HRI dataset for each study area. Due to those obvious pervious surfaces in GAIA having been removed in

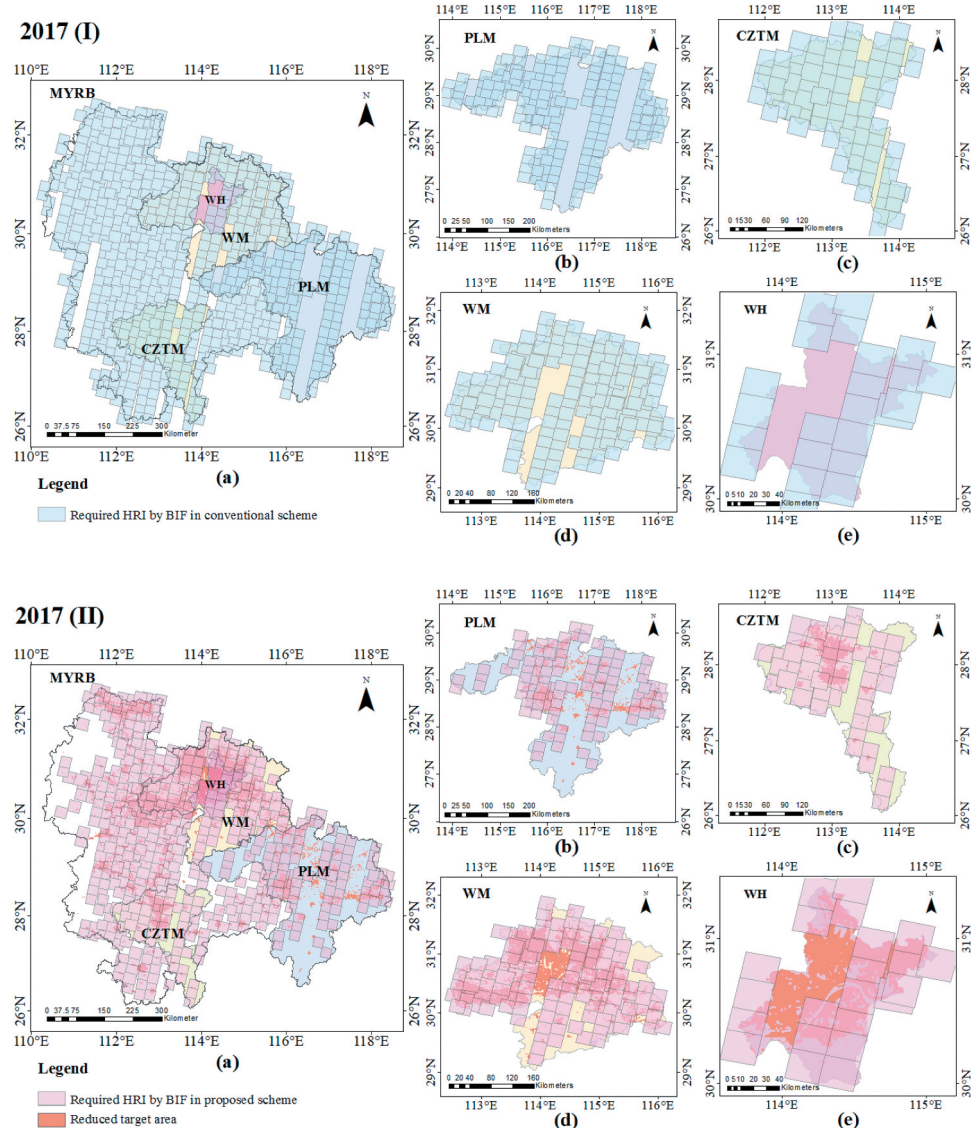


Figure 8b. HRI requirements in five study areas from 2016 to 2018: (I) the conventional full HRI scheme, (II) the proposed on-demand HRI scheme.

morphology-based target study area reduction were regarded as the pervious surfaces in the final result, the final coverage of the high-resolution impervious surface result in the total study area would be raised dramatically in the proposed scheme. That is the reason why the coverage rates on the total study area in (Table 5) are higher than the conventional scheme in (Table 4). In the result of the on-demand HRI scheme as (Table 5), there are 12 in 15 cases having coverage rate more than 95%, 14 in 15 cases with coverage rate more than 90%. Only 1 case at WH in 2017 resulted from rare HRI resources (only 33 scenes) and low HRI coverage (66.26%) of the original dataset as in (Table 1). Even in that case, there was still

5.89% coverage higher than the conventional scheme. In the 12 cases of large scale, the on-demand HRI scheme showed high performance in coverage that all 12 cases achieved coverage higher than 93%, while only 4 cases reaching more than 90% in the conventional full HRI scheme.

In order to compare the performance of the proposed and conventional scheme more specifically, a comparison was generated in two aspects as absolute difference and relative difference. As shown in (Table 6), five indicators were utilized to describe the absolute and relative differences of performance in HRI requirement and coverage. Absolute differences of the on-demand HRI scheme were the increment in

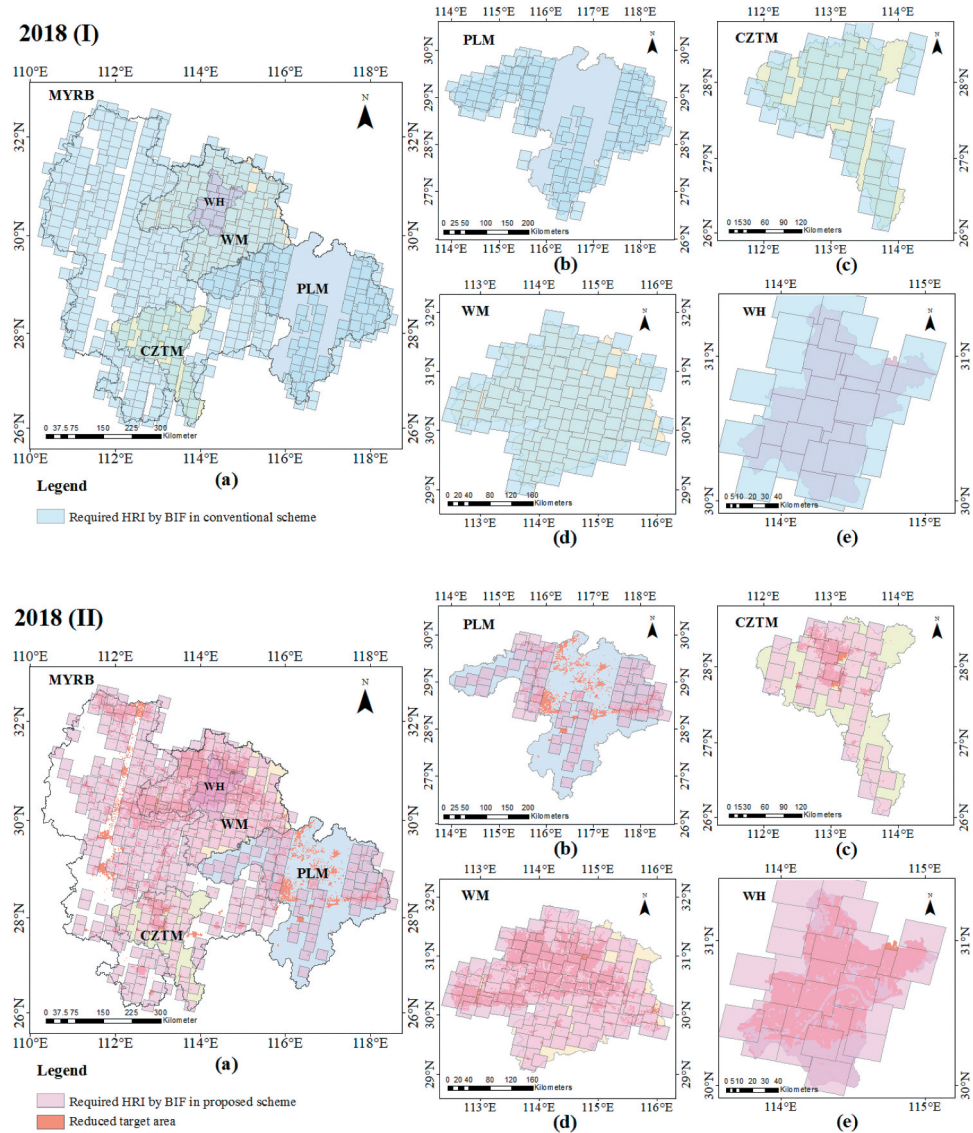


Figure 8c. HRI requirements in five study areas from 2016 to 2018: (I) the conventional full HRI scheme, (II) the proposed on-demand HRI scheme.

required HRI amount, HRI required rate, and coverage rate, where the references are the original HRI dataset and total study area. Regarding the results derived from the conventional full HRI scheme as a reference, relative differences of the proposed on-demand HRI scheme were relative ratios, including the relative HRI required rate and relative coverage rate.

In the large-scale area as urban agglomeration, the proposed on-demand HRI scheme can further reduce 239–251 scenes of HRI, decrease about 18% of HRI required rate on the original dataset, and improve about 14% of coverage rate on the total study area, where relative HRI required rate and relative coverage rate reach about –30% and 17%, respectively, when

compared with the results from the conventional scheme. At regional megalopolises, it could further diminish dozens of the HRI requirements and increase tens of the percentage of coverage. PLM performed best among the three regional megalopolises, with 28% absolute and 41% relative annual further reduced HRI required rate, further promoting 24% absolute and 37% relative annual coverage rate. Under the on-demand HRI scheme, CZTM further reduced 28% absolute and 45% relative annual HRI required rate, further improved about 11% absolute and about 13% relative annual coverage rate. With 4% absolute and 8% relative annual further reduced HRI required rate, WM increased 4.5% absolute and 5%

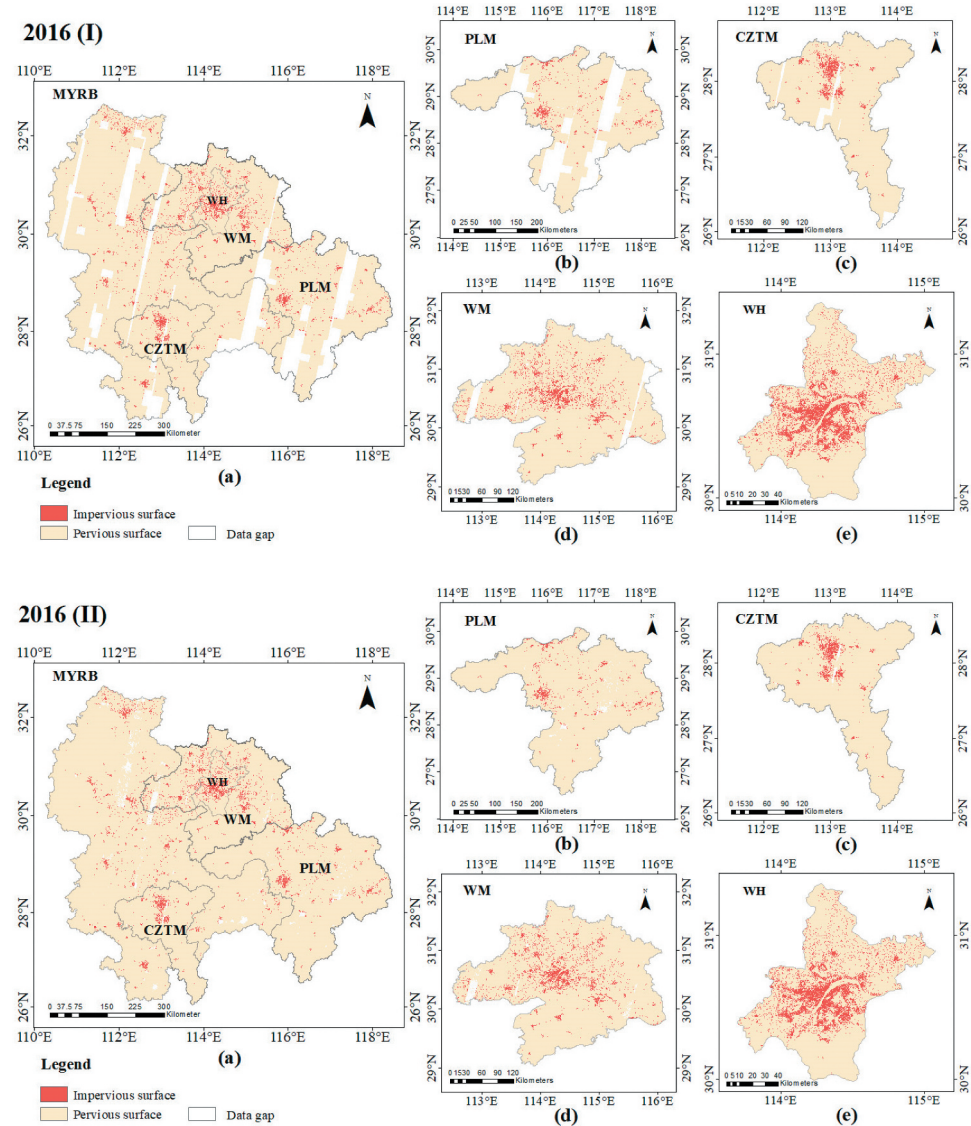


Figure 9a. High-resolution impervious surface results in five study areas from 2016 to 2018: (I) the conventional full HRI scheme, (II) the proposed on-demand HRI scheme.

relative annual coverage rate compared with the conventional scheme. As for the small scale as a city, WH further reduced 3% absolute and 8% relative annual HRI required rate, improved 2% absolute and 3% relative annual coverage rate by the on-demand HRI scheme.

The superiority of the proposed on-demand HRI scheme has been shown obviously in four large-scale areas, by comparing the indicators in (Table 6). However, there were 0 and 0.01% improvement of coverage in WH 2016 and 2018 respectively, because there left nearly no room for improvement as it had been achieved 100% and 99.56% coverage under the conventional scheme. But even in that situation, the

on-demand HRI scheme reduced the HRI requirement. The real internal reason for the performance difference between large and small scales is the design idea derived from the geospatial distribution characteristics, where lower PIS and higher aggregation will bring in more significant performance in HRI requirement and coverage. In all four large-scale areas, the PIS are less than 10% and HGADI more than 0.95. However, at the city scale, WH has a high PIS equaling 16.5% and relatively low HGADI equaling 0.9285. Furthermore, MYRB, PLM, and CZTM have a very low PIS of less than 5% and extremely high HGADI of more than 0.98, which contribute to better effects than WM. In a word, the on-demand HRI

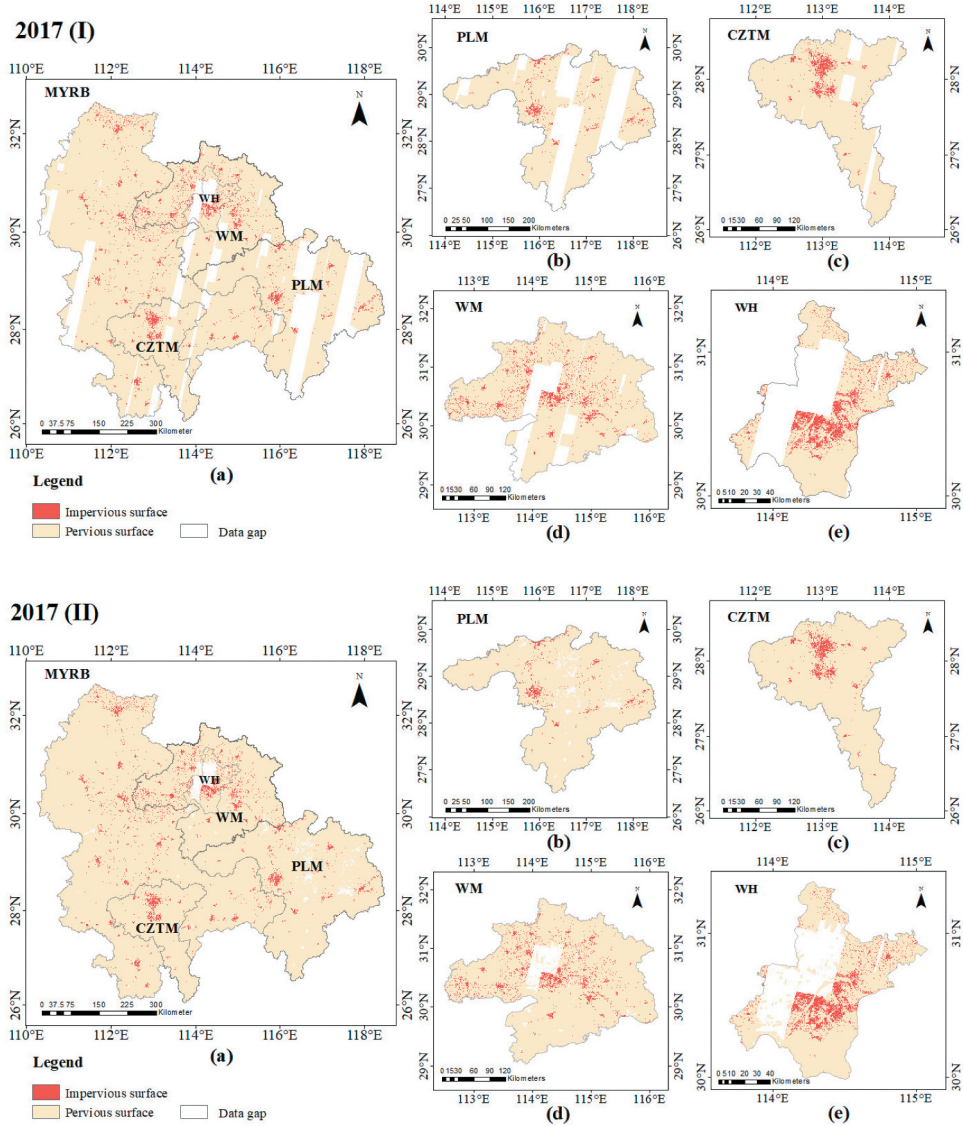


Figure 9b. High-resolution impervious surface results in five study areas from 2016 to 2018: (I) the conventional full HRI scheme, (II) the proposed on-demand HRI scheme.

scheme has the ability to reduce the demand for HRI while ensuring coverage in mapping large-scale high-resolution impervious surface, and the obvious effect and superiority will be easier appeared in large scale areas with low PIS and high geospatial aggregation.

5.3 Results of mapping large-scale high-resolution impervious surface

Based on the selected HRI, 0.8-meter high-resolution impervious surfaces were extracted from Gaofen 2 images scene by scene. The object-oriented method was followed as (Lu, Hetrick, and Moran 2011) for both proposed on-demand HRI and conventional full

HRI scheme. After result mosaicking, the final sub-meter level high-resolution impervious surface maps were generated as shown in (Figure 9). There are obvious data gaps in the result of the conventional full HRI scheme, especially in large-scale areas, shown as 2016(I), 2017(I), and 2018(I) in (Figure 9). Data gaps were significantly reduced in the results of the proposed on-demand HRI scheme, as 2016(II), 2017(II), and 2018(II) in (Figure 9). Data gaps uncovered by available data were calculated for both conventional and proposed scheme, shown in (Table 7). With smaller data gaps in all cases, the on-demand HRI scheme showed a better performance in the perspective of data integrity. The largest data gap appeared in PLM

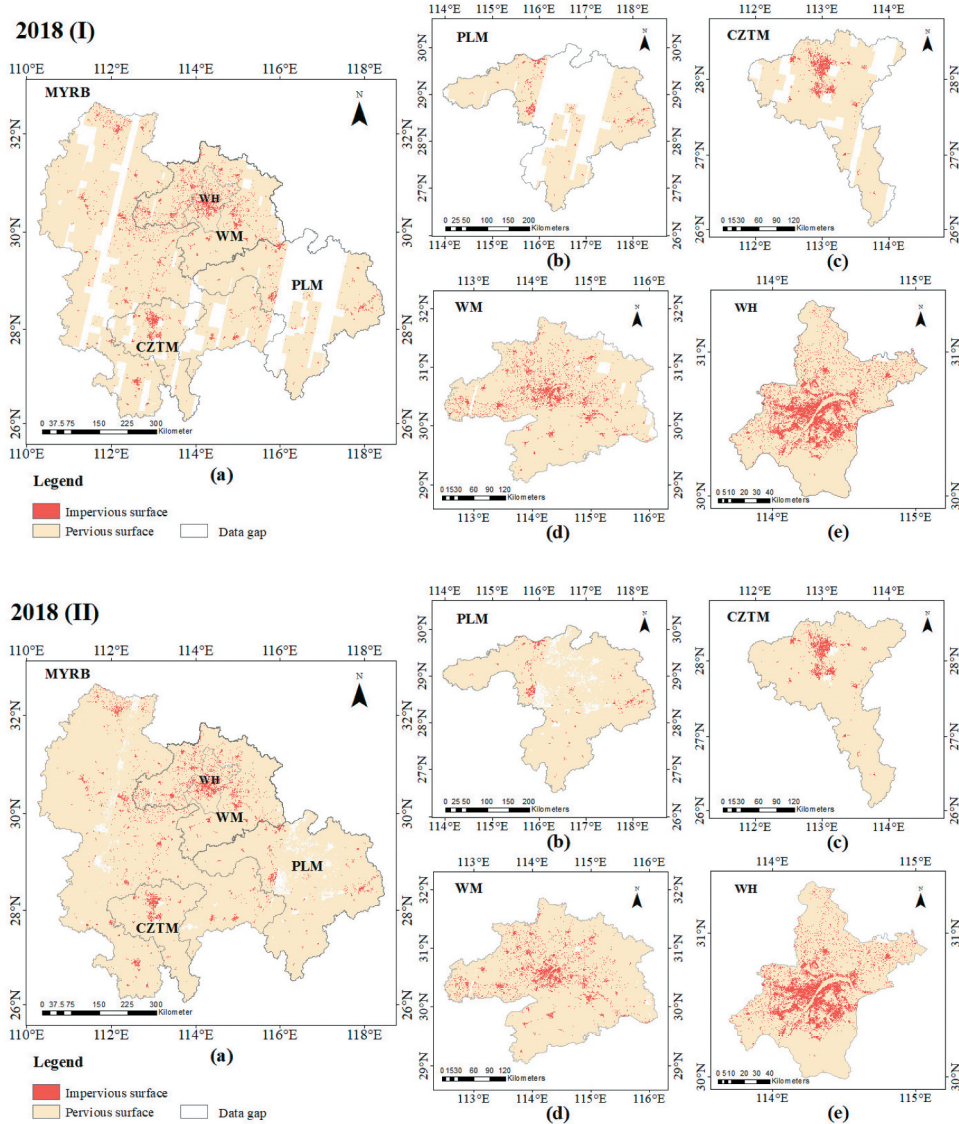


Figure 9c. High-resolution impervious surface results in five study areas from 2016 to 2018: (I) the conventional full HRI scheme, (II) the proposed on-demand HRI scheme.

2018, where the data gap rate equals 41.35% conventional scheme and 6.11% in the proposed scheme. In 12 cases at large scales, there are 10 cases having data gap rate less than 5% and 2 cases in 5–7% under the proposed on-demand HRI scheme, whereas there are only 3 cases with data gap rate less than 5%, 1 case in 5–10%, 4 cases in 10–20%, 3 cases in 20–30%, and 1 case in 40–50% under the conventional full HRI scheme. In 3 cases at city scale, the data gap rates of the two schemes are at the same level. Taking the result of the conventional scheme as a reference, a relative improvement rate was utilized to depict the improvement of the proposed on-demand HRI scheme on the basis of the conventional on-demand

HRI scheme. From the relative improvement rate in (Table 7), it is easy to find that the improvement of the on-demand HRI scheme is more significant at large scales with the improvement rate in 59.53–99.54%, rather than small scale as a city with the improvement rate in 0–17.46%.

Mapping accuracy is directly related to the classification algorithm for extracting impervious surfaces from remote sensing images. In this study, the goal is to explore geospatial distribution characteristics of impervious surface at large scales and gain the geospatial distribution knowledge from medium-resolution impervious surface data, use it to select HRI where it is really needed, and thereby reduces

Table 4. HRI requirement and coverage of the final high-resolution mapping result based on the conventional full HRI scheme.

Scales	Regions	Years	Required HRI amounts by BIF (scenes)	HRI required rates on original dataset (%)	Coverage rates on study area (%)
National urban agglomeration	MYRB	2016	853	59.61	87.14
		2017	805	59.28	84.98
Regional megalopolis	PLM	2018	783	56.13	79.27
		2016	226	69.33	86.27
		2017	189	70.52	71.94
	CZTM	2018	172	65.65	58.65
		2016	101	57.06	95.47
		2017	88	66.67	91.26
	WM	2018	90	61.22	79.85
		2016	196	41.09	95.94
		2017	167	54.93	86.84
		2018	180	48.13	96.52
City	WH	2016	41	24.26	100
		2017	23	69.70	66.26
		2018	38	44.71	99.56

The highlighted are coverage rates with value higher than 90%.

the demand for HRI and use a smaller amount of HRI while ensuring coverage in mapping high-resolution impervious surface at large scales. The focus of this study is not to design a novel classification algorithm to detect impervious surfaces from HRI, where there only uses the existing powerful and widely used method to generate the high-resolution impervious surface from HRI scene by scene. In this experiment, the object-oriented method followed as (Lu, Hetrick, and Moran 2011) has a high performance and accuracy in extracting high-resolution impervious surfaces from HRI, and was adopted in both proposed on-demand HRI and conventional full HRI scheme. As utilizing the same method for high-resolution impervious surface generation from HRI, high-resolution impervious surface results would be the same in those regions where the same HRI was chosen by both proposed and conventional scheme. The difference in the results of the proposed and conventional scheme was that only those large obvious pervious surfaces identified by the morphology-based target study area reduction method were protected and directly used in the final results of the proposed scheme. In this situation, the accuracy of the large-scale high-resolution impervious surface results should be at the same level for both proposed and conventional scheme. Additionally, the visual performance of the high-resolution impervious surface result shows in some typical areas. To scrutinize impervious surface results in detail, three subsets of representative areas are selected to show the high-resolution impervious surface result, as shown in (Figure 10). For all three regions, those impervious

surfaces were depicted in detail. Especially for typical impervious surfaces (overpass, station, and dense residential area) as the yellow bordered area in (Figure 10 (a)), they were all successfully identified as impervious surfaces without any impurities as shown in (Figure 10 (b)). It shows a high performance of the adopted method in extracting impervious surfaces from HRI.

5.4 Advantages, applicability, and limitations

Narrowing the target study area by a morphology-based method and selecting necessary HRI by BIF strategy, the proposed on-demand HRI scheme can only use HRI where it is really needed, select HRI on-demand, and thereby reduce the demand for HRI. The proposed on-demand HRI scheme uses a smaller amount of HRI while ensuring coverage, and has fewer gaps in the result, and thereby improve the efficiency of mapping high-resolution impervious surface at large scales. Fundamentally, those advantages are derived from the geospatial distribution knowledge of low overall proportion and high geospatial aggregation found in impervious surface at large scales. The effect of the proposed on-demand HRI scheme relies on the degree of the PIS and HGADI.

In principle, low overall proportion and high geospatial aggregation in the medium-resolution impervious surface product guarantees the high performance of the on-demand HRI scheme for mapping high-resolution impervious surface at large scales. In application, those study areas with PIS < 10% and HGADI > 0.9 have the potential to utilize the on-demand HRI scheme for high-resolution mapping. Furthermore, PIS < 5% and HGADI

Table 5. HRI requirement and coverage of the final high-resolution mapping result based on the proposed on-demand HRI scheme.

Scales	Regions	Years	Required HRI by BIF (scenes)	HRI required rates on original dataset (%)	Coverage rates on total study area (%)
National urban agglomeration	MYRB	2016	609	42.56	98.63
		2017	554	40.80	98.19
		2018	544	39.00	97.36
Regional megalopolis	PLM	2016	139	42.64	99.29
		2017	111	41.42	97.06
		2018	99	37.79	93.89
	CZTM	2016	56	31.64	99.50
		2017	51	38.64	99.96
		2018	47	31.97	99.05
	WM	2016	153	32.08	98.69
		2017	130	42.76	94.65
		2018	143	38.24	99.49
City	WH	2016	37	21.89	100
		2017	22	66.67	72.15
		2018	34	40.00	99.57

The highlighted are coverage rates with value higher than 90%.

> 0.95 would be highly recommended to achieve significant performance.

The proposed on-demand HRI scheme would have low applicability and suitability in the single city or smaller areas. On the one hand, the PIS would be high, especially for a prosperous big city, such as WH with PIS equaling 16.50%. The reduction rate on WH was only 34.52%, much smaller than in national urban agglomeration and regional megalopolis, resulting in the poor performance in HRI requirement and coverage. On the other hand, the coverage of a single HRI is not small when compared in a small-scale area, for example, one scene of Gaofen 2 image covering about 500 km² region. The results and analysis in Section 5.1–5.3 also confirm the high performance in large-scale areas, and low applicability at a small scale.

Additionally, the design of the on-demand HRI scheme can not only be applied in the impervious surface mapping, but also be utilized in other land cover mapping only if it features low overall proportion and high geospatial aggregation, such as water surface mapping.

There are still several limitations as listed as below:

- (1) Reliability on the performance of Step1 medium-resolution impervious surface preparation from MRI. All subsequent steps in the on-demand HRI scheme would be directly affected by the result of Step 1.
- (2) There still exists some data gaps in the final large-scale high-resolution result, although it

has been greatly improved. More other sourced remotely sensed data are required to fill the gaps, such as unmanned aerial vehicle data.

- (3) In this experiment, only Gaofen 2 was utilized as HRI to achieve sub-meter high-resolution impervious surface mapping for large-scale application. The number of sub-meter level resolution HRI imagery is quite limited, but there are dozens of meter-level HRI can be utilized to generate meter-level mapping application.

6 Conclusion

This study aimed to use information and knowledge obtained from medium-resolution impervious surface data to assist in mapping high-resolution impervious surface at large scales. Geospatial distribution knowledge from medium-resolution remotely sensed impervious surface product was explored from two perspectives: one is to analyze overall PIS in the global perspective; the other is to compare the geospatial aggregation phenomenon of the impervious surface with the surroundings from a local perspective, where HGADI was proposed to describe the geospatial aggregation from the remote sensing product which is a raster type of data. The knowledge of low overall proportion and high geospatial aggregation in impervious surface was discovered at large scales. Under the guidance of the geospatial distribution knowledge above, this study believes that HRI is not

Table 6. Absolute and relative performance of proposed on-demand HRI scheme in HRI requirement and coverage, compared with the results of conventional full HRI scheme.

Scales	Regions	Years	Required HRI amount (scenes)	Absolute differences		Relative improvement on HRI required rates (%)	Relative differences on coverage rates (%)
				HRI required rates on original dataset (%)	Coverage rates on total study area (%)		
National urban agglomeration	MYRB	2016	-244	-17.05	+11.49	-28.6	+13.19
		2017	-251	-18.48	+13.21	-31.18	+15.54
		2018	-239	-17.13	+18.09	-30.52	+22.82
Regional megalopolis	PLM	2016	-87	-26.69	+13.02	-38.5	+15.09
		2017	-78	-29.1	+25.12	-41.27	+34.92
		2018	-73	-27.86	+35.24	-42.44	+60.08
CZTM	CZTM	2016	-45	-25.42	+4.03	-44.55	+4.22
		2017	-37	-28.03	+8.7	-42.05	+9.54
		2018	-43	-29.25	+19.2	-47.78	+24.04
WM	WM	2016	-43	-9.01	+2.75	-21.94	+2.86
		2017	-37	-12.17	+7.81	-22.16	+8.99
		2018	-37	-9.89	+2.97	-20.56	+3.08
City	WH	2016	-4	-2.37	0	-9.76	0
		2017	-1	-3.03	+5.89	-4.35	+8.88
		2018	-4	-4.71	+0.01	-10.53	+0.01

Table 7. The comparison in data gap rate of the high-resolution impervious surface results.

Scales	Regions	Years	Data gap rates of full HRI scheme (%)	Data gap rates of on-demand HRI scheme (%)	Relative improvement rates (%)
National urban agglomeration	MYRB	2016	12.86	1.37	89.35
		2017	15.02	1.81	87.95
		2018	20.73	2.64	87.26
Regional megalopolis	PLM	2016	13.73	0.71	94.83
		2017	28.06	2.94	89.52
		2018	41.35	6.11	85.22
	CZTM	2016	4.53	0.5	88.96
		2017	8.74	0.04	99.54
		2018	20.15	0.95	95.29
	WM	2016	4.06	1.31	67.73
		2017	13.16	5.35	59.35
		2018	3.48	0.51	85.34
City	WH	2016	0	0	0
		2017	33.74	27.85	17.46
		2018	0.44	0.43	2.27

The highlighted are the data gap rates with value less than 5%.

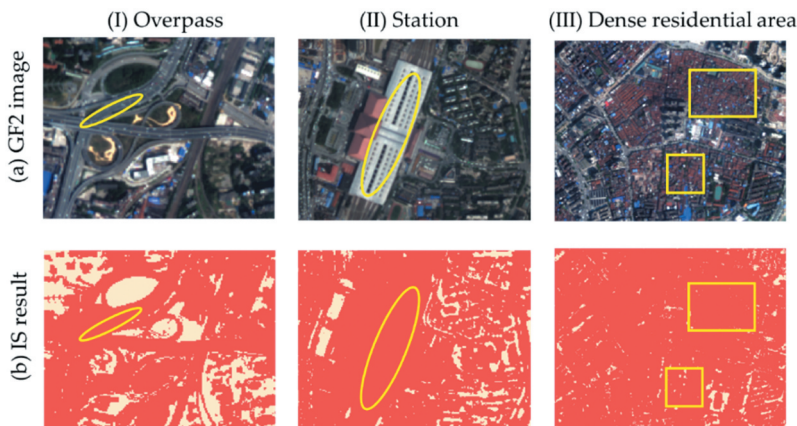


Figure 10. The high-resolution impervious surface result in three typical subsets of the study area: (I) overpass, (II) station, and (III) dense residential area. The rows are: (a) the Gaofen 2 (GF2) satellite image and (b) the impervious surface (IS) result. In row (b), color in red and orange are impervious and pervious surfaces, respectively.

necessary for the total area at large scales, such as large obvious forest and lake, which is different from the conventional full HRI scheme requiring a large amount of HRI for entire large areas.

The proposed on-demand HRI scheme can find the places with the real requirement for HRI by morphology-based target study area reduction method, select necessary HRI by BIF strategy, and thereby achieve the aim of reducing the demand for HRI while ensuring coverage in mapping large-scale high-resolution impervious surface. The experiments were implemented in 15 cases, including five study areas in three scales and each year from 2016 to 2018. The results and discussion show the high performance of

the proposed on-demand HRI scheme which can use a smaller requirement of HRI resources while ensuring coverage, and have fewer data gaps in the high-resolution results for the total large area. Compared with the small scale as a single city, the performance of the on-demand HRI scheme is more significant at large scales.

The geospatial distribution knowledge of low overall proportion and high geospatial aggregation in the medium-resolution impervious surface product guarantees the high performance of the proposed on-demand HRI scheme. In application, those study areas with PIS < 10% and HGADI > 0.9 have the potential to utilize the on-demand HRI scheme for high-resolution mapping. Furthermore,

PIS < 5% and HGADI > 0.95 would be highly recommended to be implemented, where it will achieve significant performance. Additionally, the on-demand HRI scheme has the potential to be applied in mapping other land cover types at large scales.

Acknowledgements

We appreciate the constructive suggestions and comments from the editor and anonymous reviewers.

Disclosure statement

No potential conflict of interest was reported by the authors.

Funding

This research was supported by the National Key R&D Program [2018YFB2100500], the Fundamental Research Funds for the Central Universities [2042020kf0011], National Natural Science Foundation of China program [41890822, 41771422 and 41971351] and Creative Research Groups of Natural Science Foundation of Hubei Province of China [2016CFA003].

ORCID

Min Huang  <http://orcid.org/0000-0002-2107-9227>
Wenying Du  <http://orcid.org/0000-0002-3202-5128>

References

- Baker, M. E., M. L. Schley, and J. O. Sexton. 2019. "Impacts of Expanding Impervious Surface on Specific Conductance in Urbanizing Streams." *Water Resources Research* 55 (8): 6482–6498. doi:[10.1029/2019WR025014](https://doi.org/10.1029/2019WR025014).
- Benediktsson, J. A., M. Pesaresi, and K. Arnason. 2003. "Classification and Feature Extraction for Remote Sensing Images from Urban Areas Based on Morphological Transformations." *IEEE Transactions on Geoscience and Remote Sensing* 41 (9): 1940–1949. doi:[10.1109/TGRS.2003.814625](https://doi.org/10.1109/TGRS.2003.814625).
- Bian, J. H., A. N. Li, J. Q. Zuo, G. B. Lei, Z. J. Zhang, and X. Nan. 2019. "Estimating 2009–2017 Impervious Surface Change in Gwadar, Pakistan Using the HJ-1A/B Constellation, GF-1/2 Data, and the Random Forest Algorithm." *Isprs International Journal of Geo-Information* 8 (10): 10. doi:[10.3390/ijgi8100443](https://doi.org/10.3390/ijgi8100443).
- Bramhe, V. S., S. K. Ghosh, and P. K. Garg. 2019. "Extraction of Built-up Areas from Landsat-8 OLI Data Based on Spectral-textural Information and Feature Selection Using Support Vector Machine Method." *Geocarto International* 35 (10): 1067–1087. doi:[10.1080/10106049.2019.1566406](https://doi.org/10.1080/10106049.2019.1566406).
- Cai, C., P. J. Li, and H. R. Jin. 2016. "Extraction of Urban Impervious Surface Using Two-Season WorldView-2 Images: A Comparison." *Photogrammetric Engineering And Remote Sensing* 82 (5): 335–349. doi:[10.14358/PERS.82.5.335](https://doi.org/10.14358/PERS.82.5.335).
- Chen, J., J. Chen, A. Liao, X. Cao, L. Chen, X. Chen, H. Chaoying, et al. 2015. "Global Land Cover Mapping at 30m Resolution: A POK-based Operational Approach." *Isprs Journal of Photogrammetry and Remote Sensing* 103 :7–27. doi:[10.1016/j.isprsjprs.2014.09.002](https://doi.org/10.1016/j.isprsjprs.2014.09.002).
- Chen, T., J. C. Trinder, and R. Q. Niu. 2017. "Object-Oriented Landslide Mapping Using ZY-3 Satellite Imagery, Random Forest and Mathematical Morphology, for the Three-Gorges Reservoir, China." *Remote Sensing* 9 (2): 4. doi:[10.3390/rs10010004](https://doi.org/10.3390/rs10010004).
- Corbane, C., M. Pesaresi, T. Kemper, A. J. Panagiotis Politis, V. S. Florczyk, M. Melchiorri, F. Sabo, and P. Soille. 2019. "Automated Global Delineation of Human Settlements from 40 Years of Landsat Satellite Data Archives." *Big Earth Data* 3 (2): 140–169. doi:[10.1080/20964471.2019.1625528](https://doi.org/10.1080/20964471.2019.1625528).
- Dahiya, S., P. K. Garg, and M. K. Jat. 2019. "Automated Extraction of Slum Built-up Areas from Multispectral Imageries." *Journal of the Indian Society of Remote Sensing* 48 (1): 113–119. doi:[10.1007/s12524-019-01066-7](https://doi.org/10.1007/s12524-019-01066-7).
- Deng, C. B., and Z. Zhu. 2020. "Continuous Subpixel Monitoring of Urban Impervious Surface Using Landsat Time Series." *Remote Sensing of Environment* 238: 110929. doi:[10.1016/j.rse.2018.10.011](https://doi.org/10.1016/j.rse.2018.10.011).
- Feng, M., and L. Xin. 2020. "Land Cover Mapping toward Finer Scales." *Science Bulletin* 65 (19): 1604–1606. doi:[10.1016/j.scib.2020.06.014](https://doi.org/10.1016/j.scib.2020.06.014).
- Feng, S. S., and F. L. Fan. 2019. "A Hierarchical Extraction Method of Impervious Surface Based on NDVI Thresholding Integrated with Multispectral and High-Resolution Remote Sensing Imageries." *Ieee Journal of Selected Topics in Applied Earth Observations and Remote Sensing* 12 (5): 1461–1470. doi:[10.1109/JSTARS.2019.2909129](https://doi.org/10.1109/JSTARS.2019.2909129).
- Gong, P., H. Liu, M. Zhang, L. Congcong, J. Wang, H. Huang, N. Clinton, et al. 2019. "Stable Classification with Limited Sample: Transferring a 30-m Resolution Sample Set Collected in 2015 to Mapping 10-m Resolution Global Land Cover in 2017." *Science Bulletin* 64 (6): 370–373. doi:[10.1016/j.scib.2019.03.002](https://doi.org/10.1016/j.scib.2019.03.002).
- Gong, P., L. Xuecao, J. Wang, Y. Bai, B. Chen, H. Tengyun, X. Liu, et al. 2020. "Annual Maps of Global Artificial Impervious Area (GAIA) between 1985 and 2018." *Remote Sensing of Environment* 236 :111510. doi:[10.1016/j.rse.2019.111510](https://doi.org/10.1016/j.rse.2019.111510).
- Homer, C., J. Dewitz, S. Jin, G. Xian, C. Costello, P. Danielson, L. Gass, et al. 2020. "Conterminous United States Land Cover Change Patterns 2001–2016 from the 2016 National Land Cover Database." *Isprs Journal of Photogrammetry and Remote Sensing* 162 :184–199. doi:[10.1016/j.isprsjprs.2020.02.019](https://doi.org/10.1016/j.isprsjprs.2020.02.019).

- Hu, X. F., and Q. H. Weng. 2011. "Impervious Surface Area Extraction from IKONOS Imagery Using an Object-based Fuzzy Method." *Geocarto International* 26 (1): 3–20. doi:[10.1080/10106049.2010.535616](https://doi.org/10.1080/10106049.2010.535616).
- Huang, M., N. C. Chen, W. Y. Du, Z. Q. Chen, and J. Y. Gong. 2018. "DMBLC: An Indirect Urban Impervious Surface Area Extraction Approach by Detecting and Masking Background Land Cover on Google Earth Image." *Remote Sensing* 10 (5): 5. doi:[10.3390/rs10050766](https://doi.org/10.3390/rs10050766).
- Huang, X., Y. F. Cai, and J. Y. Li. 2019. "Evidence of the Mitigated Urban Particulate Matter Island (UPI) Effect in China during 2000–2015." *Science of the Total Environment* 660: 1327–1337. doi:[10.1016/j.scitotenv.2019.01.099](https://doi.org/10.1016/j.scitotenv.2019.01.099).
- Huang, X., X. Han, M. Song, T. Lin, and J. Gong. 2019. "Monitoring Ecosystem Service Change in the City of Shenzhen by the Use of High-resolution Remotely Sensed Imagery and Deep Learning." *Land Degradation & Development* 30 (12): 1490–1501. doi:[10.1002/ldr.3337](https://doi.org/10.1002/ldr.3337).
- Hung, C. L. J., L. A. James, and M. E. Hodgson. 2018. "An Automated Algorithm for Mapping Building Impervious Areas from Airborne LiDAR Point-cloud Data for Flood Hydrology." *Giscience & Remote Sensing* 55 (6): 793–816. doi:[10.1016/j.rse.2018.02.055](https://doi.org/10.1016/j.rse.2018.02.055).
- Khare, P., J. Machesky, R. Soto, M. He, A. A. Presto, and D. R. Gentner. 2020. "Asphalt-related Emissions are a Major Missing Nontraditional Source of Secondary Organic Aerosol Precursors." *Science Advances* 6 (36): eabb9785. doi:[10.1126/sciadv.abb9785](https://doi.org/10.1126/sciadv.abb9785).
- Kuang, W., S. Zhang, X. Li, and D. Lu. 2020. "A 30-meter Resolution Dataset of China's Urban Impervious Surface Area and Green Space Fractions, 2000–2018." *Earth Syst. Sci. Data Discuss* 2020: 1–23. doi:[10.5194/essd-2020-107](https://doi.org/10.5194/essd-2020-107).
- Li, G. Y., L. W. Li, D. S. Lu, W. Guo, and W. H. Kuang. 2020. "Mapping Impervious Surface Distribution in China Using Multi-source Remotely Sensed Data." *Giscience & Remote Sensing* 57 (4): 543–552. doi:[10.1080/15481603.2020.1744240](https://doi.org/10.1080/15481603.2020.1744240).
- Li, H. B., and J. G. Wu. 2004. "Use and Misuse of Landscape Indices." *Landscape Ecology* 19 (4): 389–399. doi:[10.1023/B:LAND.0000030441.15628.d6](https://doi.org/10.1023/B:LAND.0000030441.15628.d6).
- Lin, Y. Y., H. S. Zhang, H. Lin, P. E. Gamba, and X. P. Liu. 2020. "Incorporating Synthetic Aperture Radar and Optical Images to Investigate the Annual Dynamics of Anthropogenic Impervious Surface at Large Scale." *Remote Sensing of Environment* 242: :111757. doi:[10.1016/j.rse.2020.111757](https://doi.org/10.1016/j.rse.2020.111757).
- Liu, D. D., N. C. Chen, X. Zhang, C. Wang, and W. Y. Du. 2020. "Annual Large-scale Urban Land Mapping Based on Landsat Time Series in Google Earth Engine and OpenStreetMap Data: A Case Study in the Middle Yangtze River Basin." *Isprs Journal of Photogrammetry and Remote Sensing* 159: 337–351. doi:[10.1016/j.isprsjprs.2019.11.021](https://doi.org/10.1016/j.isprsjprs.2019.11.021).
- Liu, X., H. Guohua, Y. Chen, L. Xia, X. Xiaocong, L. Shaoying, F. Pei, and S. Wang. 2018. "High-resolution Multi-temporal Mapping of Global Urban Land Using Landsat Images Based on the Google Earth Engine Platform." *Remote Sensing of Environment* 209: 227–239. doi:[10.1016/j.rse.2018.02.055](https://doi.org/10.1016/j.rse.2018.02.055).
- Lu, D., and Q. Weng. 2009. "Extraction of Urban Impervious Surfaces from an IKONOS Image." *International Journal of Remote Sensing* 30 (5): 1297–1311. doi:[10.1080/01431160802508985](https://doi.org/10.1080/01431160802508985).
- Lu, D. S., S. Hetrick, and E. Moran. 2011. "Impervious Surface Mapping with Quickbird Imagery." *International Journal of Remote Sensing* 32 (9): 2519–2533. doi:[10.1080/01431161003698393](https://doi.org/10.1080/01431161003698393).
- Meraner, A., P. Ebel, X. X. Zhu, and M. Schmitt. 2020. "Cloud Removal in Sentinel-2 Imagery Using a Deep Residual Neural Network and SAR-optical Data Fusion." *Isprs Journal of Photogrammetry and Remote Sensing* 166: 333–346. doi:[10.1016/j.isprsjprs.2020.05.013](https://doi.org/10.1016/j.isprsjprs.2020.05.013).
- Misra, M., D. Kumar, and S. Shekhar. 2020. "Assessing Machine Learning Based Supervised Classifiers For Built-Up Impervious Surface Area Extraction From Sentinel-2 Images." *Urban Forestry & Urban Greening* 53: 126714. doi:[10.1016/j.ufug.2020.126714](https://doi.org/10.1016/j.ufug.2020.126714).
- Mountakis, G., J. Im, and C. Ogole. 2011. "Support Vector Machines in Remote Sensing: A Review." *Isprs Journal of Photogrammetry and Remote Sensing* 66 (3): 247–259. doi:[10.1016/j.isprsjprs.2010.11.001](https://doi.org/10.1016/j.isprsjprs.2010.11.001).
- Patidar, N., and A. K. Keshari. 2020. "A Rule-based Spectral Unmixing Algorithm for Extracting Annual Time Series of Sub-pixel Impervious Surface Fraction." *International Journal of Remote Sensing* 41 (10): 3970–3992. doi:[10.1080/01431161.2019.1711243](https://doi.org/10.1080/01431161.2019.1711243).
- Schumaker, N. H. 1996. "Using Landscape Indices to Predict Habitat Connectivity." *Ecology* 77 (4): 1210–1225. doi:[10.2307/2265590](https://doi.org/10.2307/2265590).
- Shao, Z. F., H. Y. Fu, P. Fu, and L. Yin. 2016. "Mapping Urban Impervious Surface by Fusing Optical and SAR Data at the Decision Level." *Remote Sensing* 8 (11): 11. doi:[10.3390/rs8110945](https://doi.org/10.3390/rs8110945).
- Shao, Z., Y. Zhang, X. Huang, X. Zhu, W. Liang, and B. Wan. 2018. "Mapping Impervious Surface with 2 M Using Multi-source High Resolution Remote Sensing Images." *Geomatics and Information Science of Wuhan University* 43 (12): 1909–1915. doi:[10.13203/j.whgis20180196](https://doi.org/10.13203/j.whgis20180196).
- Sugg, Z. P., T. Finke, D. C. Goodrich, M. S. Moran, and S. R. Yool. 2014. "Mapping Impervious Surfaces Using Object-oriented Classification in a Semiarid Urban Region." *Photogrammetric Engineering and Remote Sensing* 80 (4): 343–352. doi:[10.14358/PERS.80.4.343](https://doi.org/10.14358/PERS.80.4.343).
- Tang, F., and X. Hanqiu. 2017. "Impervious Surface Information Extraction Based on Hyperspectral Remote Sensing Imagery." *Remote Sensing* 9 (6): 5506. doi:[10.3390/rs9060550](https://doi.org/10.3390/rs9060550).
- Tang, P. F., Z. L. Miao, C. Lin, P. J. Du, and S. C. Guo. 2020. "An Automatic Method for Impervious Surface Area Extraction by Fusing High-resolution Night Light and Landsat OLI Images." *Journal of Infrared and Millimeter Waves* 39 (1): 128–136.
- Tobler, W. R. 1970. "A Computer Movie Simulating Urban Growth in the Detroit Region." *Economic Geography* 46 (sup1): 234–240. doi:[10.2307/143141](https://doi.org/10.2307/143141).
- Wang, P., C. Huang, E. C. Brown, J. C. T. De Colstoun, and B. Tan. 2017. *Global Human Built-up and Settlement Extent (HBASE) Dataset from Landsat*. Palisades, NY: NASA Socioeconomic Data and Applications Center (SEDAC).

- Wang, Y. L., and M. S. Li. 2019. "Urban Impervious Surface Detection from Remote Sensing Images A Review of the Methods and Challenges." *Ieee Geoscience and Remote Sensing Magazine* 7 (3): 64–93. doi:10.1109/MGRS.2019.2927260.
- Weng, Q. 2012. "Remote Sensing of Impervious Surfaces in the Urban Areas: Requirements, Methods, and Trends." *Remote Sensing of Environment* 117: 34–49. doi:10.1016/j.rse.2011.02.030.
- Xu, H., and M. Wang. 2016. "Remote Sensing-based Retrieval of Ground Impervious Surfaces."
- Xu, H. Q., M. Y. Wang, T. T. Shi, H. D. Guan, C. Y. Fang, and Z. L. Lin. 2018. "Prediction of Ecological Effects of Potential Population and Impervious Surface Increases Using a Remote Sensing Based Ecological Index (RSEI)." *Ecological Indicators* 93: 730–740. doi:10.1016/j.ecolind.2018.05.055.
- Xu, R. D., J. Liu, and J. H. Xu. 2018. "Extraction of High-Precision Urban Impervious Surfaces from Sentinel-2 Multispectral Imagery via Modified Linear Spectral Mixture Analysis." *SENSORS* 18: 9.
- Xu, Z. W., G. Mountakis, and L. J. Quackenbush. 2017. "Impervious Surface Extraction in Imbalanced Datasets: Integrating Partial Results and Multi-temporal Information in an Iterative One-class Classifier." *International Journal of Remote Sensing* 38 (1): 43–63. doi:10.1080/01431161.2016.1259677.
- Yu, H. F., Y. L. Zhao, and Y. C. Fu. 2019. "Optimization of Impervious Surface Space Layout for Prevention of Urban Rainstorm Waterlogging: A Case Study of Guangzhou, China." *International Journal of Environmental Research and Public Health* 16 (19): 19. doi:10.3390/ijerph16193613.
- Yu, X. J., Z. F. Shen, X. Cheng, L. G. Xia, and J. C. Luo. 2016. "Impervious Surface Extraction Using Coupled Spectral-spatial Features." *Journal of Applied Remote Sensing* 10 (3): 1–14. doi: 10.1117/1.JRS.10.035013.
- Zhang, L., and Q. H. Weng. 2016. "Annual Dynamics of Impervious Surface in the Pearl River Delta, China, from 1988 to 2013, Using Time Series Landsat Imagery." *Isprs Journal of Photogrammetry and Remote Sensing* 113: 86–96. doi:10.1016/j.isprsjprs.2016.01.003.
- Zhang, L., M. Zhang, and Y. B. Yao. 2018. "Mapping Seasonal Impervious Surface Dynamics in Wuhan Urban Agglomeration, China from 2000 to 2016." *International Journal of Applied Earth Observation and Geoinformation* 70: 51–61. doi:10.1016/j.jag.2018.04.005.
- Zhang, T., and X. Huang. 2018. "Monitoring of Urban Impervious Surfaces Using Time Series of High-Resolution Remote Sensing Images in Rapidly Urbanized Areas: A Case Study of Shenzhen." *Ieee Journal of Selected Topics in Applied Earth Observations and Remote Sensing* 11 (8): 2692–2708. doi:10.1109/JSTARS.2018.2804440.
- Zhang, X., L. Y. Liu, C. S. Wu, X. D. Chen, Y. Gao, S. Xie, and B. Zhang. 2020. "Development of a Global 30m Impervious Surface Map Using Multisource and Multitemporal Remote Sensing Datasets with the Google Earth Engine Platform." *Earth System Science Data* 12 (3): 1625–1648. doi:10.5194/essd-12-1625-2020.
- Zhu, C. Y., J. Li, S. Q. Zhang, C. S. Wu, B. Zhang, L. R. Gao, and A. Plaza. 2018. "Impervious Surface Extraction from Multispectral Images via Morphological Attribute Profiles Based on Spectral Analysis." *Ieee Journal of Selected Topics in Applied Earth Observations and Remote Sensing* 11 (12): 4775–4790. doi:10.1109/JSTARS.2018.2877768.
- Ziter, C. D., E. J. Pedersen, C. J. Kucharik, and M. G. Turner. 2019. "Scale-dependent Interactions between Tree Canopy Cover and Impervious Surfaces Reduce Daytime Urban Heat during Summer." *Proceedings of the National Academy of Sciences of the United States of America* 116 (15):7575–7580. doi: 10.1073/pnas.1817561116.